Automatic Optimization Procedure for Stellarator Coils

M. Drevlak

IPP 2/335 February 1997

MAX-PLANCK-INSTITUT FÜR PLASMAPHYSIK

85748 GARCHING BEI MÜNCHEN

Automatic Optimization Procedure for Stellarator Coils

M. Drevlak

IPP 2/335 **February 1997**

MAX-PLANCK-INSTITUT FÜR PLASMAPHYSIK

D-85748 Garching bei München, Germany

Die nachstehende Arbeit wurde im Rahmen des Vertrages zwischen dem Max-Planck-Institut für Plasmaphysik und der Europäischen Atomgemeinschaft über die Zusammenarbeit auf dem Gebiet der Plasmaphysik durchgeführt

Abstract

The present design of the modular primary field coils for W7-X leaves only modest space between the inner cryostat wall and the last closed magnetic surface for installation of the divertor system. Therefore, two alternative coil designs aimed at increasing the volume inside the coil system were devised using an automatic optimization procedure. First a detailed outline of the requirements on the coil system and of the optimization procedure is given. Then the new coil configurations are presented and their properties compared against the original coil design. It is found that the first of the new designs has features making it attractive for a future fusion power plant, whereas the second design would be interesting for the experiment W7-X itself if found necessary due to requirements on installation space for the divertor system.

Contents

I Introduction

Stellarators confine toroidal plasmas with magnetic fields generated by currents external to the plasma. They share many features of toroidal confinement with the tokamak, but require no net toroidal plasma current. Instead, the rotational transform of the magnetic field is generated by the coil system.

The W7-X Stellarator configuration is based on the HELIAS class of optimized stellarator equilibria [1]. Here, the shapes of the magnetic flux surfaces are optimized for achieving stable confinement of the plasma at high values of $\langle\beta\rangle$ and long neoclassical energy confinement times. Moreover, confinement of α-particles with energies of 3.5 MeV, which would be produced in an actual power plant, is ensured. For W7-X a plasma configuration with 5 periods was chosen. It has a major radius of 5.5 m and is aimed at stably confining the plasma at a pressure characterized by $\langle\beta\rangle = 5\%$.

Once a desired plasma equilibrium is established, the shape of the coils must be designed to reproduce its magnetic surfaces with high precision. For W7-X the standard confinement field is generated by 10 modular superconducting coils per period, resulting in 50 primary field coils for the entire machine. Due to the stellarator symmetry, the 10 coils per machine period correspond to only 5 truly different coil shapes from which the whole machine is constructed. The coils are closed poloidally and hence can be manufactured separately. This modularity of the coil system also holds the potential for maintenance and replacement of individual coils.

It is an inherent disadvantage of modular coils that only modest space is left inside the coils for installation of a divertor system. The latter is needed to deal with particle exhaust from the plasma and is subject to a considerable heat load. In its current design the coil system for W7-X leaves only a relatively small distance between the last closed magnetic surface (LCMS) of the plasma column and the inner cryostat wall. This holds especially for the inner part of the bean shaped cross-section of the machine, where this distance reduces to values in the order of 10 cm to a few 10 cm [2]. Therefore increasing this distance would be favorable with respect to divertor installation [3].

In this context one must also consider the possibilty of space demands by the divertor increasing at a later time. Numerous fusion experiments (for instance JET or ASDEX Upgrade) have been operated not with a single divertor system but with a number of different divertor systems replacing each other. It is highly conceivable that W7-X, too, will, at some point in its

lifetime, obtain a new divertor system different from the one envisaged by the current machine design. Hence, the space available should be made as large as possible in order to ensure the potential of W7-X for such future modifications.

Considering an actual fusion power plant, the availability of space gains even greater importance, as in this case additional 1.0 to 1.5 m of space will be required for the installation of shield and blanket. For this reason, too, it would be desirable to find a configuration of coils located further away from the plasma boundary, keeping the desired plasma surface with sufficient accuracy.

In section II of this paper a detailed outline of the requirements on the coil system of a stellarator will be given and a method for arriving at an appropriate coil system will be described. Then, in section III two modified coil designs are presented, which aim at easing the space limitations for the installation of a divertor system in W7-X. It will be shown that coil configurations can be found which increase the minimum distance between the current carrying surface (CCS) and the plasma boundary by several cm while preserving the plasma configuration sufficiently well. The total coil length of the coils as well as the magnetic field energy are increased to some extent (for the geometrical prescriptions used here). In section IV finally a number of comparative views of the coil systems will be shown.

II Requirements and Approach to Coil Optimization

In this section a number of criteria on the structure of the magnetic field produced by the coil system and on the geometrical properties of the coils themselves will be described. Moreover, a procedure for optimizing a coil configuration with respect to these criteria will be outlined.

For the calculation of the properties of a coil system the finite transverse extent of the coils can be ignored. Instead, the coils will be described by the shape of their centerlines. These centerlines of the coils will henceforth be referred to as "filaments". They are represented by closed polygons.

The plasma configuration is described by a set of nested magnetic flux surfaces with toroidal topology. In order to approximate the desired shapes of these magnetic surfaces, the geometry of the coils is designed to minimize the normal component of the magnetic field on the outermost of these surfaces.

Three quantities are used to measure the transverse magnetic field on a desired magnetic surface. The local relative error of the magnetic field is defined as

$$e_l = \frac{\left|\vec{B}\cdot\vec{n}\right|}{|\vec{B}|}, \tag{1}$$

where $\vec{B}$ is the magnetic induction and $\vec{n}$ denotes the normal on the plasma surface. The average error is defined as the mean value of the local relative error over the desired plasma boundary:

$$e_a = \frac{\int_A e_l \mathrm{d}A}{A}. \tag{2}$$

Here, A denotes the area of the plasma boundary. The error of the magnetic field can also be expressed with the average squared error, which is defined as

$$e_q = \int_A \left(\vec{B}\cdot\vec{n}\right)^2 \mathrm{d}A. \tag{3}$$

The original coil configuration for W7-X [4] was found using the NESCOIL code [5]. For a given current carrying surface this code determines the distribution of the current density for which the average squared error [Eq. (3)] becomes a minimum for given total toroidal and poloidal currents. For a solution with vanishing net toroidal current this current distribution was divided toroidally into segments of equal poloidal current. These segments correspond directly to the path of the filament over the current carrying surface. Finally the resulting filament shapes were subjected to a smoothing procedure.

In this paper coil designs are presented which were obtained with an extended version of the NESCOIL code. Instead of first calculating a fourier series for the current distribution by solving an appropriate linear equation system and then partitioning this analytic current profile into discrete currents, this code finds the coil shapes by performing a nonlinear optimization of both the properties of the magnetic field and geometrical properties of the coils themselves. In the following a brief account of the parameters included in this optimization will be given.

The magnetic field of the coil system is characterized by two important integral parameters, the specific volume and the rotational transform. The specific volume of a magnetic surface is defined as the average of the line integral along a line of force of the expression $1/B$ around the machine and is expressed as the limit of

$$q = \lim_{N\to\infty} \frac{1}{N} \int_{N \text{ turns}} \frac{dl}{B} \tag{4}$$

for an infinite number of integrations around the machine axis. A radial decrease of the specific volume off the magnetic axis is commonly called "magnetic well". A magnetic well is necessary for the stability of the plasma configuration. The radial profile of the rotational transform ι on a magnetic surface is of importance in connection with the so-called resonances [1, 6].

Another parameter to be considered during the optimization is the radial deviation of the magnetic axis from its design position. It is observed that this parameter can deviate by magnitudes in the order of of 10 cm (in the case of W7-X) from its design value without leading to any significant increase of the field error. Given the space limitations inside the coil system and especially the small distance between plasma boundary and cryostat wall, deviations of the position of the axis with this magnitude cannot be accepted. Therefore this parameter must be included in the optimization.

Moreover, the magnitudes of the islands surrounding some of the fixed points of the Poincaré mapping of the magnetic lines of force can be considered. This magnitude is characterized by the residual R introduced by [9]. In the designs presented, only the islands at $\iota = 1$ were taken into account. However, other islands, too, may be included. In some applications even the residuals of fixed points located in a region with stochastic behavior of the field lines may be accounted for in order to exert control on the field structure in these domains.

In addition to reproducing the desired properties of the magnetic field, the coil system must comply with a number of geometrical constraints to be feasible with respect to engineering issues.

Firstly, since the coils will be of finite extent, the distance between adjacent filaments must not fall below a certain threshold since otherwise the coil cross-sections would intersect. Secondly, the minimum curvature radii $\rho = 1/\kappa$ of the filaments must be sufficiently large to make winding of the cable-in-conduit conductor possible.

Thirdly, unnecessary undulations of the coils should be avoided. This is important for facilitating the manufacturing process of the coils. To this purpose a measure for a weighted

curvature of a coil was introduced in [7]. It is defined as the line integral over the coil length

$$F = \frac{1}{2\pi} \int_0^L g(\kappa) \cdot \kappa(s) \mathrm{d}s \tag{5}$$

where the curvature weight g is defined as

$$g(\kappa) = \begin{cases} \frac{\kappa - \kappa_{min}}{\kappa_{max} - \kappa_{min}}, & \kappa > \kappa_{min} \\ 0 \qquad \text{else} \end{cases} \tag{6}$$

Generally, it will be desired to keep the weighted curvatures of the coils as small as possible.

For the case of W7-X the parameters κ_{min} and κ_{max} are set to the values

$$\kappa_{min} = 1/(0.65\ \mathrm{m} + r_{coil}) \tag{7}$$

$$\kappa_{max} = 1/(0.20\ \mathrm{m} + r_{coil}). \tag{8}$$

r_{coil} is a measure for the coil width, which in the computations presented here is set to a value of $r_{coil} = 0.1$ m. It is added in order to produce an estimate of the upper bound on the weighted curvature of the edges of the coil pack instead of the corresponding value for the filament itself. This is done because it is the curvature of the coil edges which is relevant for construction of the coils, since here the strongest curvatures will occur. If the weighted curvature of a given coil edge was calculated, the term r_{coil} would be omitted. The numerical values for κ_{min} and κ_{max} were established empirically, drawing upon available experience gathered in the manufacturing of stellarator coils [7]. The qualitative behavior of the curvature weight g with respect to the filament curvature κ is exemplified in Fig. 1.

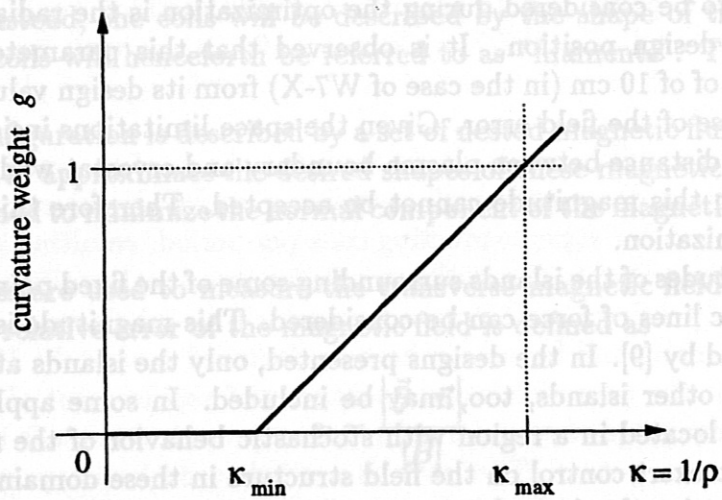

Fig. 1: Qualitative behavior of the curvature weight g with respect to the curvature κ.

In order to gain greater insight into the meaning of the weighted curvature it is instructive to consider a circle with the (trivially) constant curvature $\kappa(s) = \kappa_0$ and the associated weighted curvature $F = F_0$. It can be shown that for a distorted curve with the curvature $\tilde{\kappa}(s) = \kappa_0 + \Delta\kappa(s)$, $\oint \Delta\kappa(s)\mathrm{d}s = 0$, the resulting weighted curvature $\tilde{F}$ always satisfies $\tilde{F} \geq F_0$. Thus, for curves with identical integrated curvature $\oint \kappa \mathrm{d}s$ a difference in the weighted curvatures can be viewed as indicating differently strong deviations from a circular shape.

These requirements on the coils and their magnetic field lead to an optimization scheme, which is carried out by the extended version of the NESCOIL code. In this code the filaments, i.e. the center lines of the coil packs, are allowed to move freely on a current carrying surface, which in turn is allowed to assume shapes confined to the volume between an inner and an outer limiting surface.

The code calculates a penalty function that reflects

- the average field error [Eq. (2)] and the maximum of the local error [Eq. (1)]
- the magnetic well
- the deviation of the rotational transform ι from its design profile
- the position of the magnetic axis
- the magnitudes of magnetic islands.
- the minimum distances of adjacent coils
- the maximum filament curvatures
- the weighted filament curvature

It is computed as

$$\mathcal{P} = \sum_i w_i(x_i) \cdot \left(\frac{x_i - x_i^{design}}{x_i^{design}} \right)^2, \tag{9}$$

the sum in Eq. (9) extending over the quantites listed above. There the x_i denote the actual quantities and x_i^{design} their design values. The $w_i(x_i)$ are weight functions for each of these quantities. In general these weight functions are constants, which in some cases are set to zero during the calculation of the penalty function. This is done for instance for the contribution from the filament distances, when the distances are greater than the design value so that no penalty is contributed, or when the magnetic well is found to exceed its design value. Usually the magnitudes of the weight constants are chosen empirically as to produce contributions of similar magnitude to the penalty function from the different criteria. However, when certain properties do not approach their design values with sufficient accuracy with this choice of weight constants, the corresponding weight constants are increased to produce larger contributions to the weight function.

The optimization of the shape of the current carrying surface between the two constraining surfaces and the path of the filaments on the CCS is then performed automatically using a numerical minimization routine. By minimizing the penalty function, it will approximate the desired machine properties as closely as possible.

In principle the minimization of the field error would lead to a coil design producing the correct values for the rotational transform and magnetic well. However, inclusion of the geometric requirements will compromise the accuracy of the magnetic field. As a result, the coils obtained may produce wrong rotational transforms or insufficient magnetic wells. Therefore these important properties are included separately in the penalty function.

Generally, a single run of the extended NESCOIL code will not produce a coil configuration complying sufficiently well with all requirements. Therefore this code must be used in an iterative manner. In this procedure the coil configuration produced by the previous run of the

optimization code is subjected to a diagnosis of its geometrical and magnetic properties. Then the optimization is continued with a new run of the NESCOIL code with appropriately modified values of the weight constants, using the previouly obtained coil configuration as starting point. This procedure is repeated until the coil configuration obtained is considered satisfactory.

This approach for finding the coil shapes is significantly different from the procedure followed in [4]. Therefore, this attempt to find coils on only slightly different current carrying surfaces with a different procedure can also be viewed as a test on wether the current coil design still offers much leeway for improvements or if it has already been pushed to the point where improvements can only be obtained by making compromises on other criteria.

As a starting point for the coil optimization, one has to choose

1. the magnetic surface to be approximated by the field of the coil system and
2. an inner and an outer constraining surface between which the surface carrying the filaments may be located.

The magnetic surfaces and the surfaces constraining the CCS are usually represented as Fourier series of the form

$$r = \sum_{m,n} r_{mn} \cos\left[2\pi\left(mu + nv\right)\right] \tag{10}$$

$$z = \sum_{m,n} z_{mn} \sin\left[2\pi\left(mu + nv\right)\right] \tag{11}$$

Here, u and v are a poloidal and a toroidal parameter, each ranging from 0 to 1 to represent one period of the machine. For a system with n_p machine periods, the parameter v is linked to the azimuthal angle ϕ according to

$$\phi = 2\pi v / n_p. \tag{12}$$

Since it was the aim to find coils further away from the plasma, the new constraining surfaces were made to lie outside the current carrying surface of the present coil configuration. In the following, results relating to two different choices of constraining surfaces are presented. As the magnetic surface to be approximated, a surface outside the chain of islands with $\iota = 1$ as produced by the present coil design was used.

In the first case, which will be referred to as configuration "W7-X-A", the new constraining surfaces were generated from the current carrying surface of the present design by increasing the parameters r_{10} and z_{10} from expressions (10) and (11) by 5 cm for the inner constraining surface and by 15 cm for the outer constraining surface. For comparison: at the inner indentation of the bean shaped cross-section of the machine the distance between plasma boundary and inner cryostat wall reduces to $\sim$ 14 cm. The resulting inner and outer constraining surfaces, together with the original current carrying surface and the magnetic surface to be approximated, are displayed in Fig. 2.

The second case, which will be called the "W7-X-B" design, was produced by selectively shifting the original current carrying surface in outward direction in the regions where space for installation of the divertors is expected to be required. The magnitude of this shift was 5 cm and 10 cm for the inner and the outer constraining surfaces respectively. The resulting surfaces, again with the magnetic surface to be approximated and the original magnetic surface, are shown in Fig. 3.

The new coil designs were intended as a modification of the original coil configuration. Therefore, the original approach using 10 coils per machine period was implemented. The

optimizations of the coil geometries were carried out using 100 polygon points for the representation of each coil. Likewise all numerical results presented concerning the cases W7-X-A and W7-X-B were obtained from a representation of the filaments by 100 polygonial points each.

III Results of the Optimizations

The optimization process produced two coil configurations reproducing the original magnetic surface with sufficient accuracy. The solution for the W7-X-A case has a maximum local field error [Eq. (1)] of 5.8% and an average field error [Eq. (2)] of 1.44%. For the W7-X-B case a maximum local error of 5.1% and an average error of 1.24% are achieved.

As increasing the space between the coils and the plasma boundary was the most prominent motivation for the optimization effort, Figs. 4 to 7 show the resulting new current carrying surfaces and the last closed magnetic surfaces within the chain of the $\iota = 1$ islands in comparison with the original coil design. It can be seen that in both cases the space between the LCMS and the current carrying surface is improved by several cm.

The case of W7-X-A is now considered in greater detail. At the bean shaped cross-section a shift of the CCS away from the plasma boundary of $\sim$ 5.5 cm is measured at the inner indentation. The magnitude of the shift then remains at a value of a few cm until the inner tip of the cross-section is reached. It then rapidly increases to its maximum value of 15 cm and remains at these high values over the entire outer region of the cross-section. Proceeding from the bean shaped cross-section to the triangular cross-section of the machine, the outward shift of the CCS becomes rather uniform. Overall, a significant increase of the machine cross-section is observed.

In the case of W7-X-B, an outward shift slightly in excess of 8 cm is observed at the tips of the bean shaped cross-section. Proceeding towards the triangular cross-section of the machine, similarly large magnitudes of the shift are found in the regions sensitive to the divertor installation. At the outer tip of the triangular cross-section the shift magnitude finally reaches a value of 10 cm.

Poincaré Plots Figs. 8 to 11 show the complete Poincaré plots for the new coil designs in comparison with the original coil configuration. It can be verified that the new configurations produce field lines approximating the magnetic surfaces obtained with the present coil design with good precision. Moreover, the sizes of the islands at $\iota = 1$ are quite similar. In contrast to the other configurations, W7-X-A exhibits virtually no closed magnetic surfaces outside the islands at $\iota = 1$.

Stability considerations for the plasma configuration lead to the requirement that the magnetic well from the magnetic axis to the last magnetic surface within $\iota = 1$ must have a magnitude of $\sim$ 1%. In Fig. 12 the radial profile of the specific volume for the two cases are compared with the specific volume of the original design. In all cases the specific volume is normalized to its value on the magnetic axis. It turns out that all coil geometries produce magnetic wells of similar magnitude. The new designs both differ from the original design in that the region occupied by the islands with $\iota = 1$ commences at a slightly smaller radius. This becomes clearer in Fig. 13, where the radial profile of the rotational transform is shown. The rotational transform on the axis evaluates to $\iota = 0.867$ for W7-X-A and $\iota = 0.864$ for W7-X-B, compared with $\iota = 0.855$ produced by the original coil system. The design value for ι to be approximated by all of the configurations is $\iota = 0.86$.

From the fact that in the new designs the islands with $\iota = 1$ start at slightly smaller radii it might be suspected that for these designs the plasma volume would be reduced by $\sim$ 15%. However, this is not the case as this shift of the islands is largely due to a small inward shift of the magnetic axis. This becomes evident from Figs. 8 and 9. Moreover, Figs. 4 to 7 showed that also the aspect ratios of the new configurations are slightly different from the original

design. For these reasons the plasma volume in the new designs is, as will be outlined later, virtually identical with the volume of the original configuration.

Coil Lengths The improvement of available space between the plasma boundary and the coils goes along with a corresponding increase of the total length of the coils (for the boundary conditions used here).

The individual coil lengths for the old and the new configuration are listed in Table I for the five different coil types found in a half machine period. For the case of the W7-X-B design, the

coil	W7-X-A	original design	W7-X-B
1	9.26 m	8.55 m	8.83 m
2	9.25 m	8.48 m	8.71 m
3	9.62 m	8.48 m	8.84 m
4	9.79 m	8.52 m	8.75 m
5	9.78 m	8.48 m	8.68 m
total	47.70 m	42.51 m	43.81 m

TABLE I: Lengths of the individual coils for the case of the present design and for the new optimizations.

increase of overall coil length amounts to 3%, which is considered modest. The 12% increase in coil length for configuration W7-X-A would inflict a greater penalty in terms of construction cost. Modifications to the auxiliary coils that might become necessary with the new designs were not considered.

Filament Curvature and Distances The filaments describing the coils must comply with a number of geometric constraints so that the coils can be constructed.

First, the coils are of finite transverse extent, the lateral width occupied by the conductors being 166 mm. Allowing for a few extra cm for steel casing of the coils, one arrives at the requirement that the minimum distance between the center lines of any two coils must not drop below a value of 28 cm. The actual achieved values for filament distances for the new coil designs as well as for the original coil system are summarized in Table II. It is seen that the

coils	W7-X-A	original design	W7-X-B
0-1	28.3 cm	28.8 cm	28.3 cm
1-2	28.2 cm	28.0 cm	28.8 cm
2-3	28.1 cm	28.7 cm	30.3 cm
3-4	28.2 cm	28.7 cm	28.2 cm
4-5	28.0 cm	30.6 cm	30.6 cm
5-6	28.3 cm	30.0 cm	36.2 cm

TABLE II: Minimum distances between adjacent coils of the configuration. The new designs W7-X-A and W7-X-B are compared with the original design.

requirements on the minimum filament distances are met by all of the three configurations. For the case of the W7-X-A design however it is noted that all filament distances are very close to

the required minimum. It appears that for this case the potential for further increases of the machine volume is practically exhausted.

Next, the filament curvatures are considered. The coils are wound from superconducting cable enclosed in an aluminium jacket. The manufacturing process of the coils requires that the curvature radii of these jackets are kept above a value of $\rho = 20$ cm. In order to guarantee curvature radii of this magnitude for the conductor jackets, a boundary of the filament curvature was established at a curvature radius of $\rho = 40$ cm. The values of the minimum curvature radii of the filaments found for the three coil designs are summarized in Table III. For both of the new configurations, the smallest curvature radii encountered fall only slightly below the value of 40 cm, posing no obstacle to their construction. Again it is concluded that there is no more leeway for further increases of the cross-section of the machine.

coil	W7-X-A	original design	W7-X-B
1	43.2 cm	42.5 cm	40.9 cm
2	40.8 cm	42.5 cm	41.1 cm
3	40.7 cm	40.0 cm	38.3 cm
4	39.9 cm	42.7 cm	40.9 cm
5	39.6 cm	45.1 cm	40.5 cm

TABLE III: Minimum curvature radii $\rho = 1/\kappa$ of the 5 different coil types. The new designs W7-X-A and W7-X-B are compared with the original design.

For the weighted curvature [Eq. (5)] an upper limit of 0.3 is desired. The actual values of

coil	W7-X-A	original design	W7-X-B
1	0.288	0.262	0.281
2	0.298	0.258	0.277
3	0.297	0.294	0.311
4	0.297	0.299	0.296
5	0.312	0.221	0.296

TABLE IV: Values of the weighted curvature F according to expression (5). The new designs W7-X-A and W7-X-B are compared with the original design.

the weighted curvature found for the three coil configurations are displayed in Table IV. As was already observed for the filament distances and the maximum curvatures, the potential for further increase of the machine volume seems to be exhausted. Both of the new designs exceed the threshold of 0.3 for the weighted curvature by a very small margin, which is not prohibitive for the construction of such coils. Experience indicates [8] that the actual weighted curvatures of the edges of the coil packs are usually short of the estimated value obtained with Eq. (5) from the filaments.

Stored Field Energy The increase of the machine cross-section in the modified coil designs will by necessity infer a growth of the stored field energy. Generally, this may lead to a growth of overall system cost. The field energy was calculated by computing the complete matrix of inductances of all coils with respect to each other and then setting the coil currents to a

uniform value that produces an average magnetic induction of 2.5 T on the magnetic axis. For the calculation of the coupling inductances the coils were assumed to be infinitely thin filaments. For the computation of the self-inductances the coils were modeled as having a circular cross-section with a radius of 105 mm. The resulting area of the cross-section of 0.0345 m^2 thus is the same as the total cross-section of conducting material for the actual coils. The field energies obtained with this procedure for the different coil designs are shown in Table V. For W7-X-A

W7-X-A	original design	W7-X-B
519 MJ	428 MJ	450 MJ

TABLE V: Stored field energies for the different coil designs.

the increase of the stored energy is $\sim 21\%$, which would imply an increase in construction cost. In comparison, the 5% increase of energy encountered for W7-X-B is rather small.

Plasma Volume The plasma volume is defined as the volume enclosed by the LCMS within the island chain with $\iota = 1$. It can be calculated analytically from the Fourier representation of the LCMS defined by expressions (10) and (11).

Any modification of the coil design will lead to slight deformations of the magnetic surfaces of the configuration. As a consequence, the plasma volume may exhibit slight variations. The values of this volume for the different configurations are summarized in Table VI. The deviations

W7-X-A	original design	W7-X-B
27.97 m^3	28.48 m^3	28.26 m^3

TABLE VI: Plasma volume for the different coil designs.

of the plasma volume from the value found for the original coil design do not exceed 1.7% and are therefore considered not significant.

IV Comparative Views of the Coil Systems

In this section a number of pictures of the complete coil set and of only one period of the coil system are presented (Figs. 14 to 25). It will become evident that even in geometric details the structure of the coil shapes obtained with the new designs is very similar to that of the original configuration. Nevertheless, some small differences will become visible to the bare eye. Generally, the reader will recognize that the new coils are twisted slightly stronger and that the azimuthal excursions of the coils are a little more pronounced. In addition, the regions of closest approximation between adjacent coils are sometimes moved to other regions of the coils than in the case of the original design.

V Conclusions

The first conclusion to be drawn from this work relates to the original coil system for the W7-X according to [4]. It was found that also by adopting a fundamentally different approach to finding an appropriate coil configuration for W7-X, drastic improvements of the coil properties could not be achieved. Increases of the space available within the coils could be attained but involved slightly smaller coil distances, smaller curvature radii and larger weighted curvatures. Thus, the new W7-X-A and W7-X-B designs are very close to the limit of what is feasible for coil construction. Moreover, it may be mentioned that the optimization process for finding the new coil shapes has required a very great computational effort before coils with properties comparable to those of the original configuration were obtained. It is concluded that the original coil system already makes excellent use of the available design freedom as constrained by the geometrical requirements on the coils.

The second conclusion relates to the viability of semi-automatic optimization of the coil shapes. This approach was used successfully for finding new coil configurations for W7-X and it has produced coil geometries similar to those of the original coil system. Therefore, this method holds the potential both for rapid modifications of a coil design when made necessary by engineering requirements and for carrying out parametric studies on possible coil configurations.

The new coil configurations found with the outlined approach are of different relevance. Configuration W7-X-A is characterized by a rather uniform increase of the machine cross-section. This makes it interesting for considerations of a real power plant. There, additional space requirements arise from the neutron production, demanding a shield and a breeding blanket inside the coil system. Since a power plant is expected to be roughly four times larger than the W7-X (in its linear dimensions), the additional 5 to 15 cm gained at W7-X-A would translate into 20 to 60 cm for a typical HELIAS device [10]. The additional cost associated with the greater total coil length and stored field energy would then be inevitable anyway. The W7-X-B case might also be of interest for experimental devices, i.e. for the current W7-X project, if space requirements of the divertor system should make a slightly larger machine cross-section imperative. The W7-X-B design, by increasing the machine volume only in the sensitive regions, would infer only a very modest additional cost in terms of coil length and stored field energy.

Although not yet compromising the feasibility of the coils from the engineering point of view, the increase of machine volume had to be bargained for a small increase of coil curvatures and a tendency to slightly reduced filament distances. The impact of these marginal drawbacks may vanish completely when applicability of the new coil designs to a fusion power plant of

HELIAS type is considered. Since such a device is anticipated to have roughly four times the size of the experiment W7-X and to operate at only twice its magnetic field strength, the coils of a HELIAS type power plant will become thinner in relation to the overall machine size. In this case the limits on tolerable filament curvatures and distances could be reevaluated, giving additional freedom for the design of an appropriate coil system.

On the other hand, as a modification to the approach underlying the W7-X-B design, it might be conceivable to find coil configurations which increase the space available for the divertors without increasing the overall machine volume. This could be done by moving the coils closer to the plasma in regions where space requirements are rather relaxed, like for instance the outer side of the bean shaped cross section or at the inside of the triangular cross section. Thus the overall machine volume would only be redistributed.

The two last considerations also open the doorway to a further set of applications for the presented procedure of coil design for stellarators. Iteration of the optimization procedure with modified requirements on the coil system could be initiated with modest amount of preparation, opening a second stage of machine optimization in addition to the optimization of the plasma column itself as introduced in [1].

Acknowledgements

The author thanks P. Merkel and J. Nührenberg for their support, fruitful discussions and for reading the manuscript. Moreover, instructive conversations with J. Sapper are gratefully acknowledged. Particular gratitude is due to Ch. Hennig for assistance in producing the colored coil plots. Part of this work was performed at the Centro Svizzero di Calcolo Scientifico, Manno, under the agreement on cooperation between Centre de Recherches en Physique des Plasmas and the Max-Planck-Institut für Plasmaphysik.

References

[1] J. Nührenberg, R. Zille, "Stable Stellarators with Medium β and Aspect Ratio", Physics Letters **114A**, 3, 1986, pp. 129

[2] WENDELSTEIN Project group, "Wendelstein 7-X Phase II Application for Preferential Support", Max-Planck-Institut für Plasmaphysik, Garching, June 1994

[3] J. Junker (Ed.), "Wendelstein 7-X Application for Preferential Support, Phase II", Max-Planck-Institut für Plasmaphysik, Garching, 1995

[4] J. Kißlinger, "Modification of the W7-X Modular Coils Improving the Aspect Ratio at High Rotational Transform", Proceedings of the 6-th Workshop on Wendelstein 7-X and Helias Reactors, Schloß Ringsberg, Bavaria, 20-24 Nov. 1995

[5] P. Merkel, "Solution of Stellarator Boundary Value Problems with External Currents", Nuclear Fusion, vol. 27, No. 5 (1987), pp. 867

[6] A. I. Morozov, L. S. Solov'ev, "The Structure of Magnetic Fields", Reviews of Plasma Physics, vol. 2, Consultants Bureau, New York, 1966, pp. 1

[7] J. Sapper, private communication

[8] P. Merkel, private communication

[9] J. M. Greene, "Two-Dimensional Measure Preserving Mappings", J. Math. Phys., vol. 9, number 5, May 1968, pp. 760

[10] C. Beidler et al., "Reactor Studies on Advanced Stellarators", Plasma Physics and Controlled Nuclear Fusion Research, fourteenth conference proceedings, 1992, Würzburg, Germany, pp. 327

W7-X-A

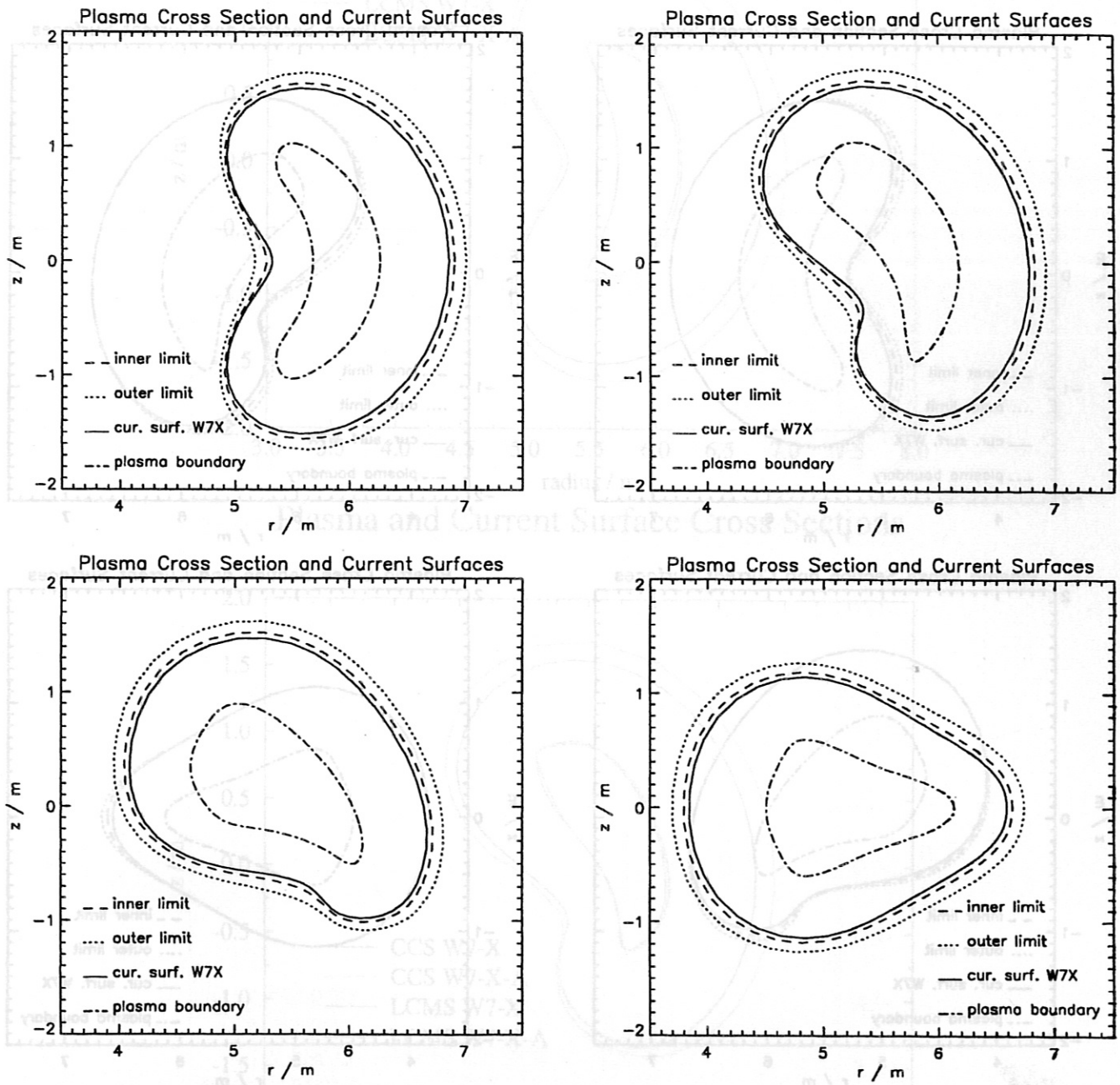

Fig. 2: Inner constraining surface (dashed line) and outer constraining surface (dotted line) of configuration W7-X-A for the optimization of the coil shapes, shown at different cross-sections of the machine. Both were chosen to be outside the original current carrying surface (solid line) in order to increase the distance between coil pack and plasma boundary. In addition the desired plasma boundary, i.e. the magnetic surface to be approximated by the optimization, is drawn (dash-dots). It is one of the first closed magnetic surfaces outside $\iota = 1$.

W7-X-B

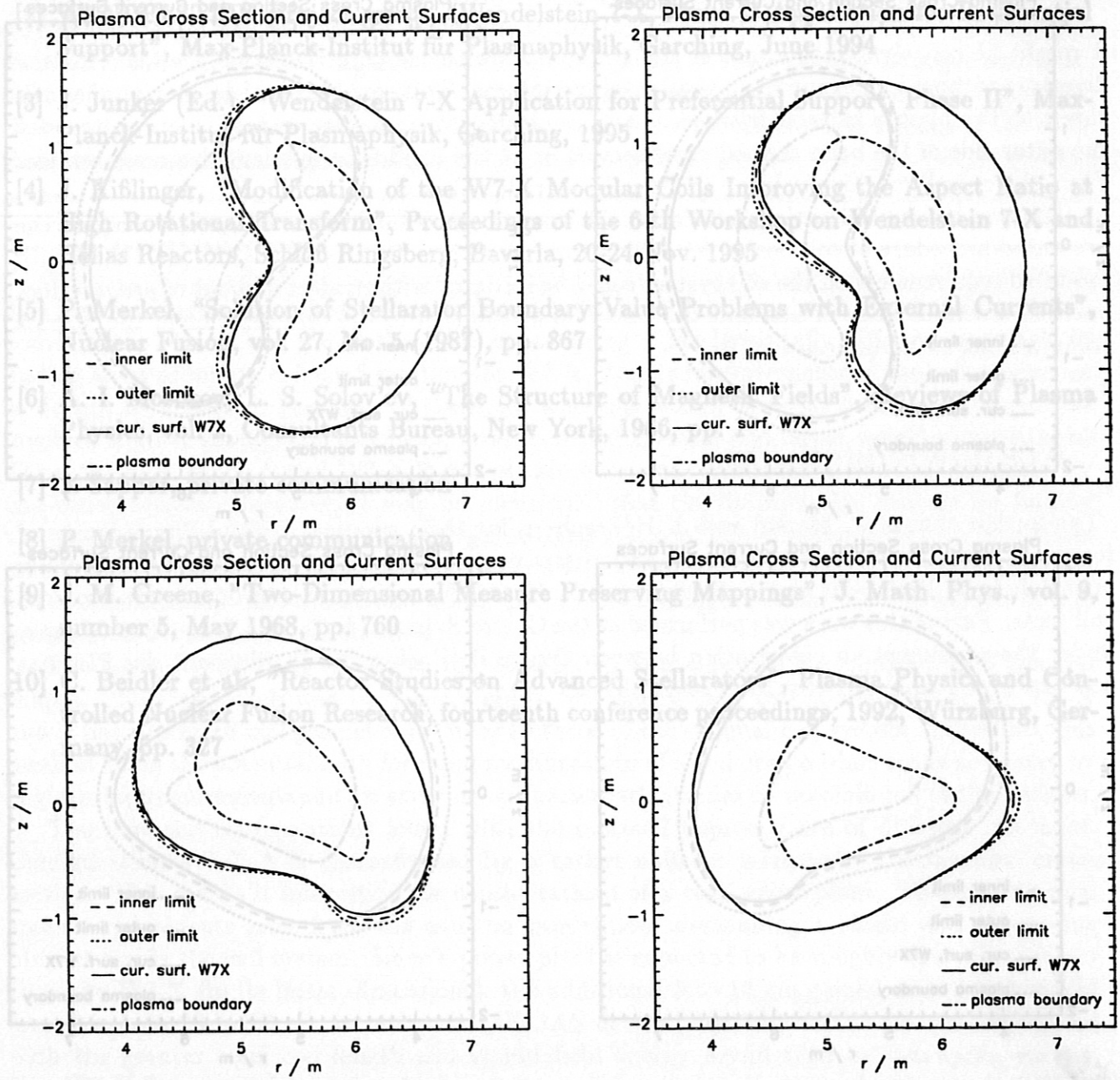

Fig. 3: Inner constraining surface (dashed line) and outer constraining surface (dotted line) of configuration W7-X-B for the optimization of the coil shapes, shown at different cross-sections of the machine. Both were chosen to be outside the original current carrying surface (solid line) in order to increase the distance between coil pack and plasma boundary. In addition the desired plasma boundary, i.e. the magnetic surface to be approximated by the optimization, is drawn (dash-dots). It is one of the first closed magnetic surfaces outside $\iota = 1$.

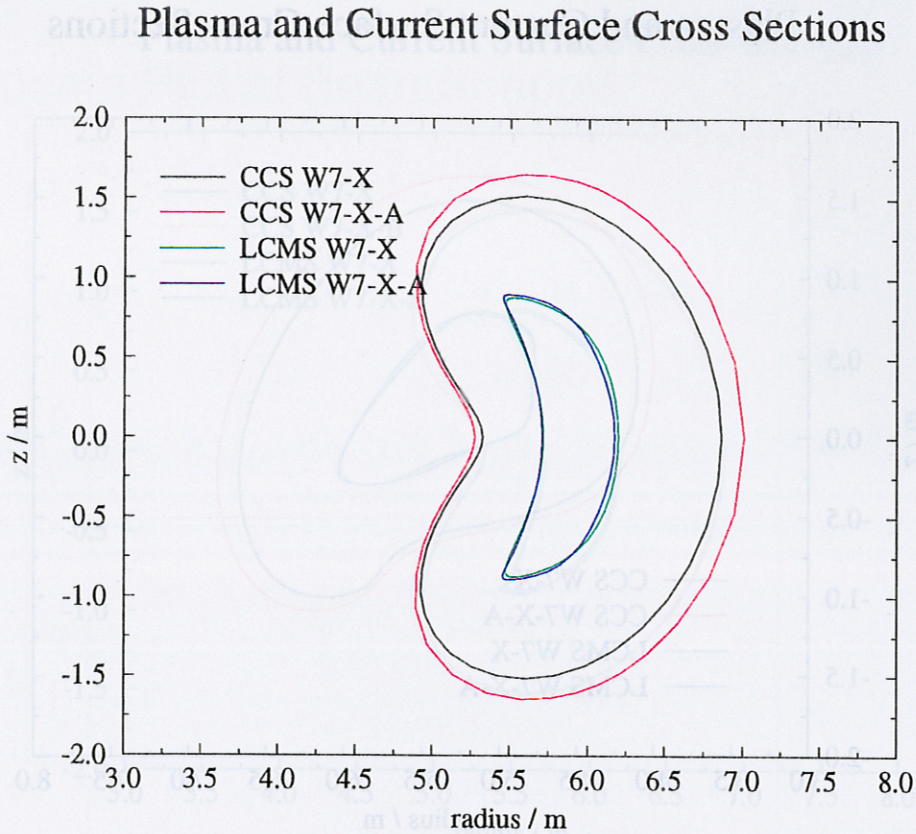

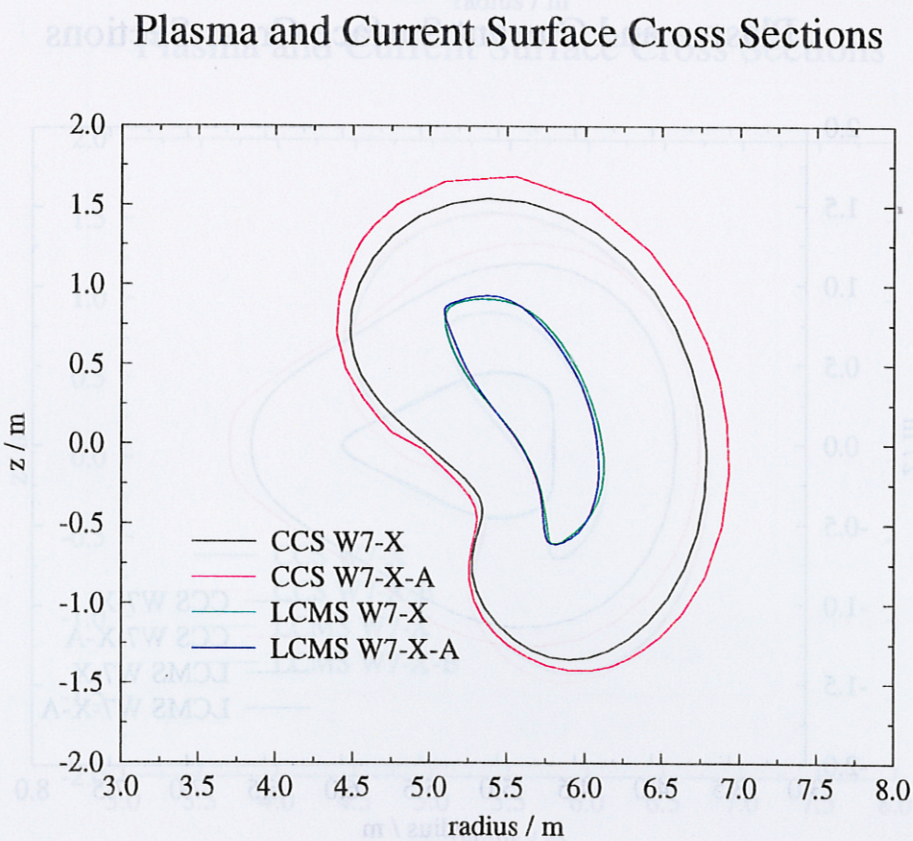

Fig. 4: Comparison of the current carrying surfaces (CCS) and the last closed magnetic surfaces (LCMS) found within $\iota < 1$ for the original coil system (W7-X) and the modified design W7-X-A.

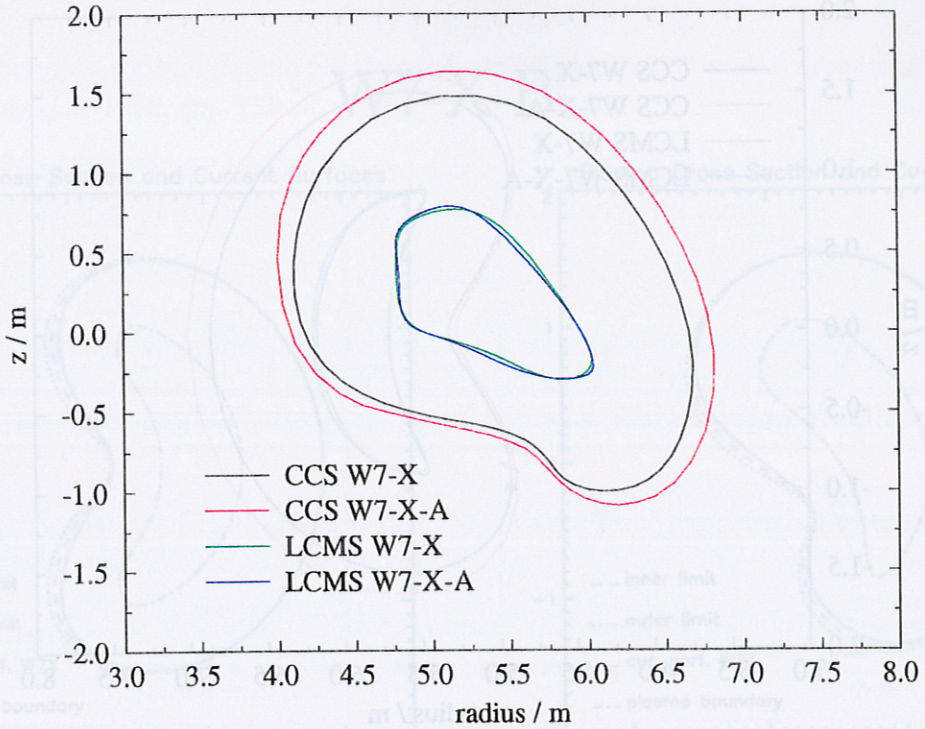

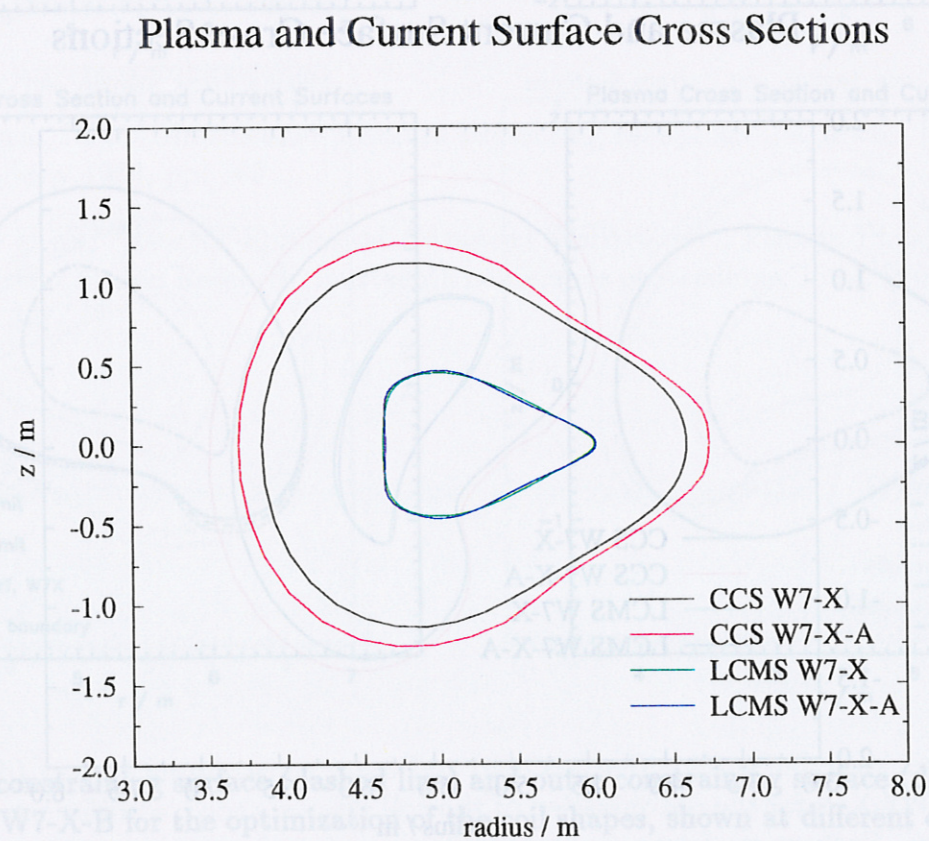

Fig. 5: Comparison of the current carrying surfaces (CCS) and the last closed magnetic surfaces (LCMS) found within $\iota < 1$ for the original coil system (W7-X) and the modified design W7-X-A.

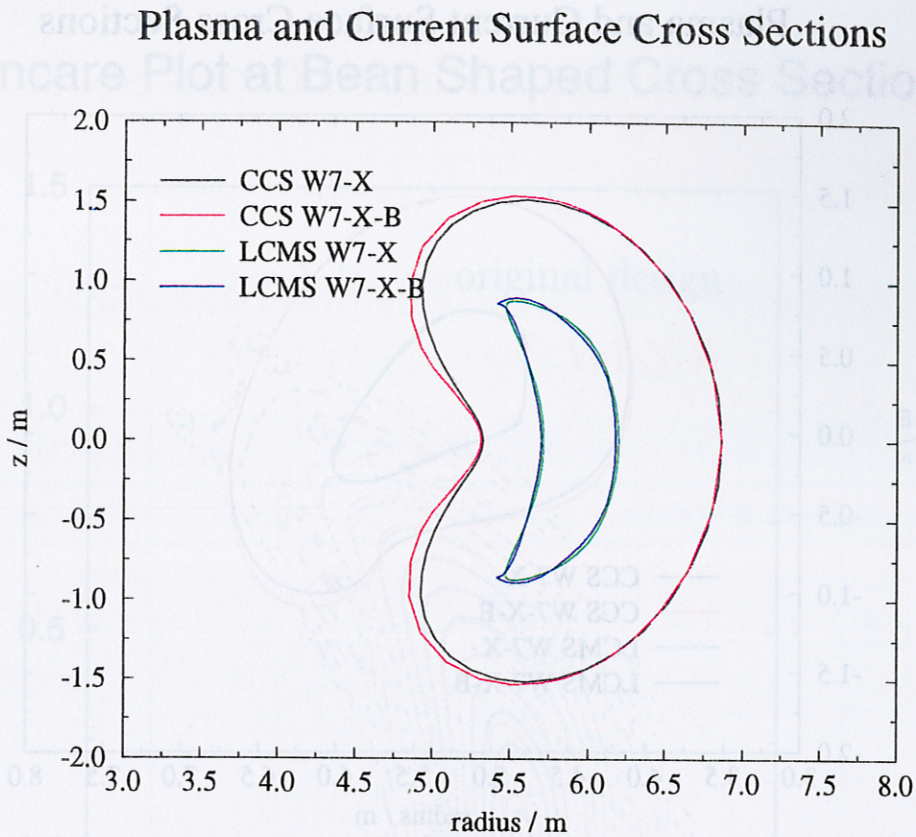

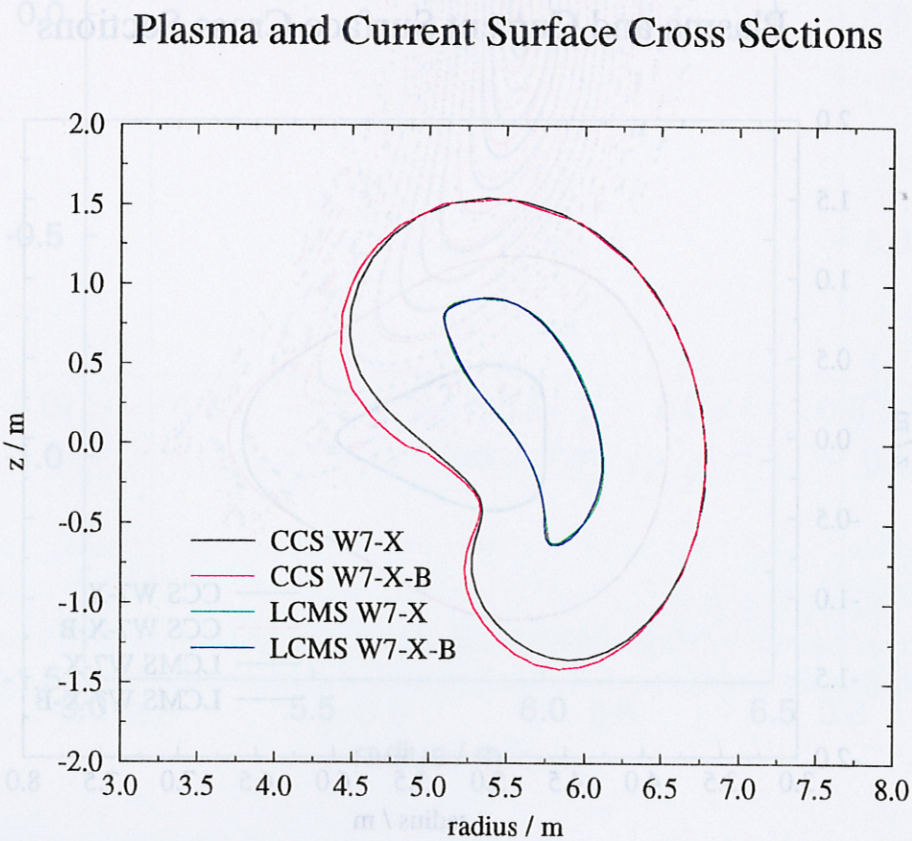

Fig. 6: Comparison of the current carrying surfaces (CCS) and the last closed magnetic surfaces (LCMS) with $\iota < 1$ for the original coil system (W7-X) and the modified design W7-X-B.

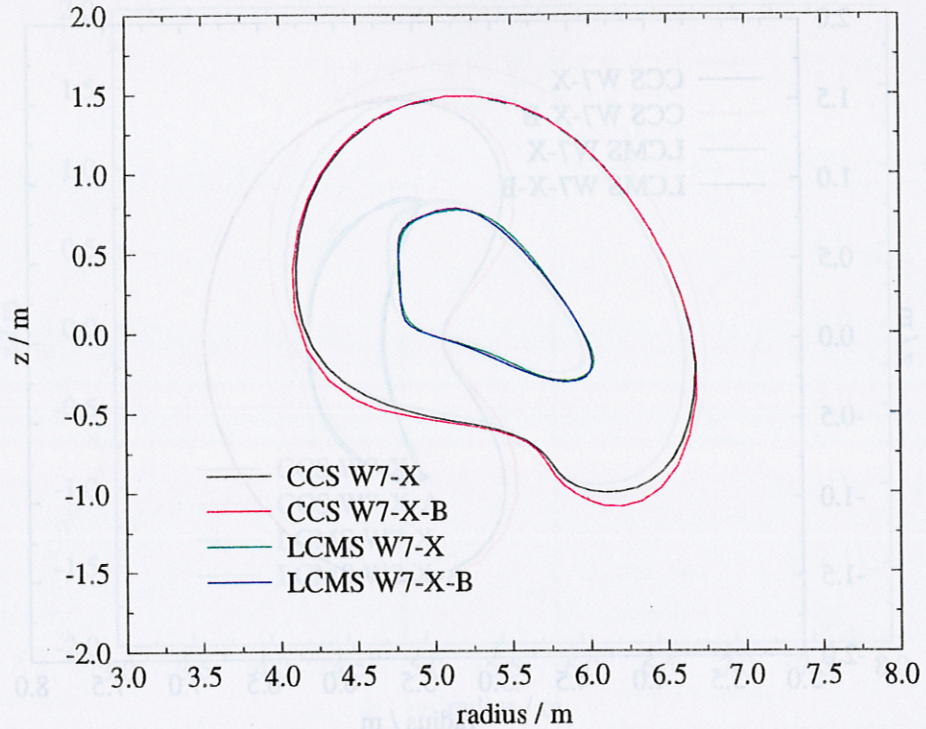

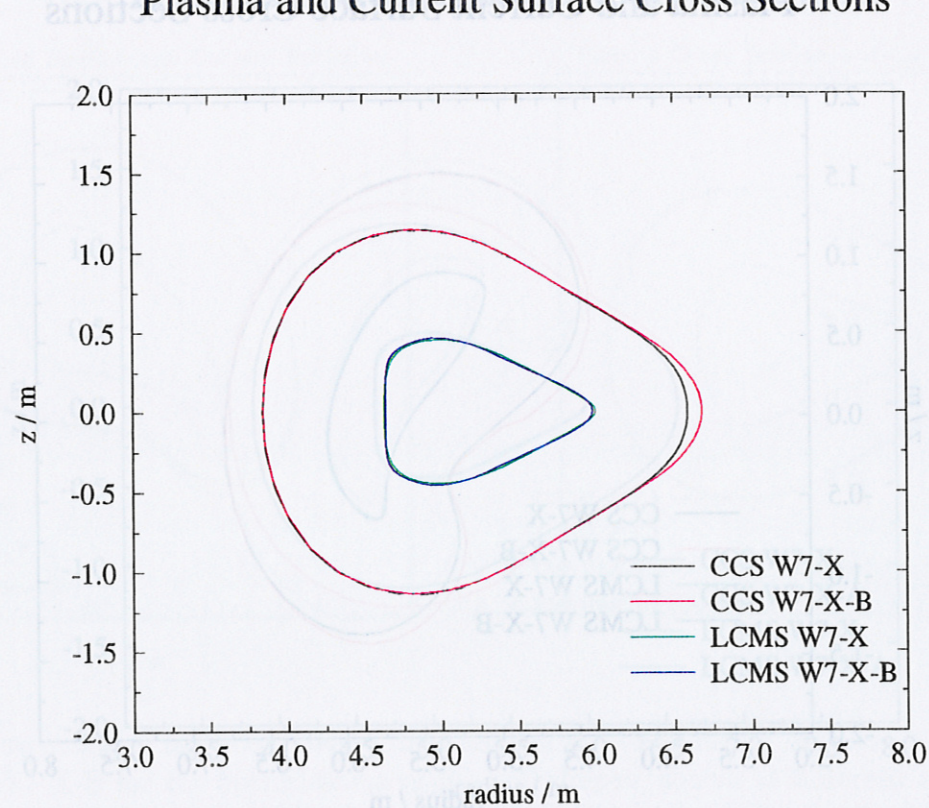

Fig. 7: Comparison of the current carrying surfaces (CCS) and the last closed magnetic surfaces (LCMS) with $\iota < 1$ for the original coil system (W7-X) and the modified design W7-X-B.

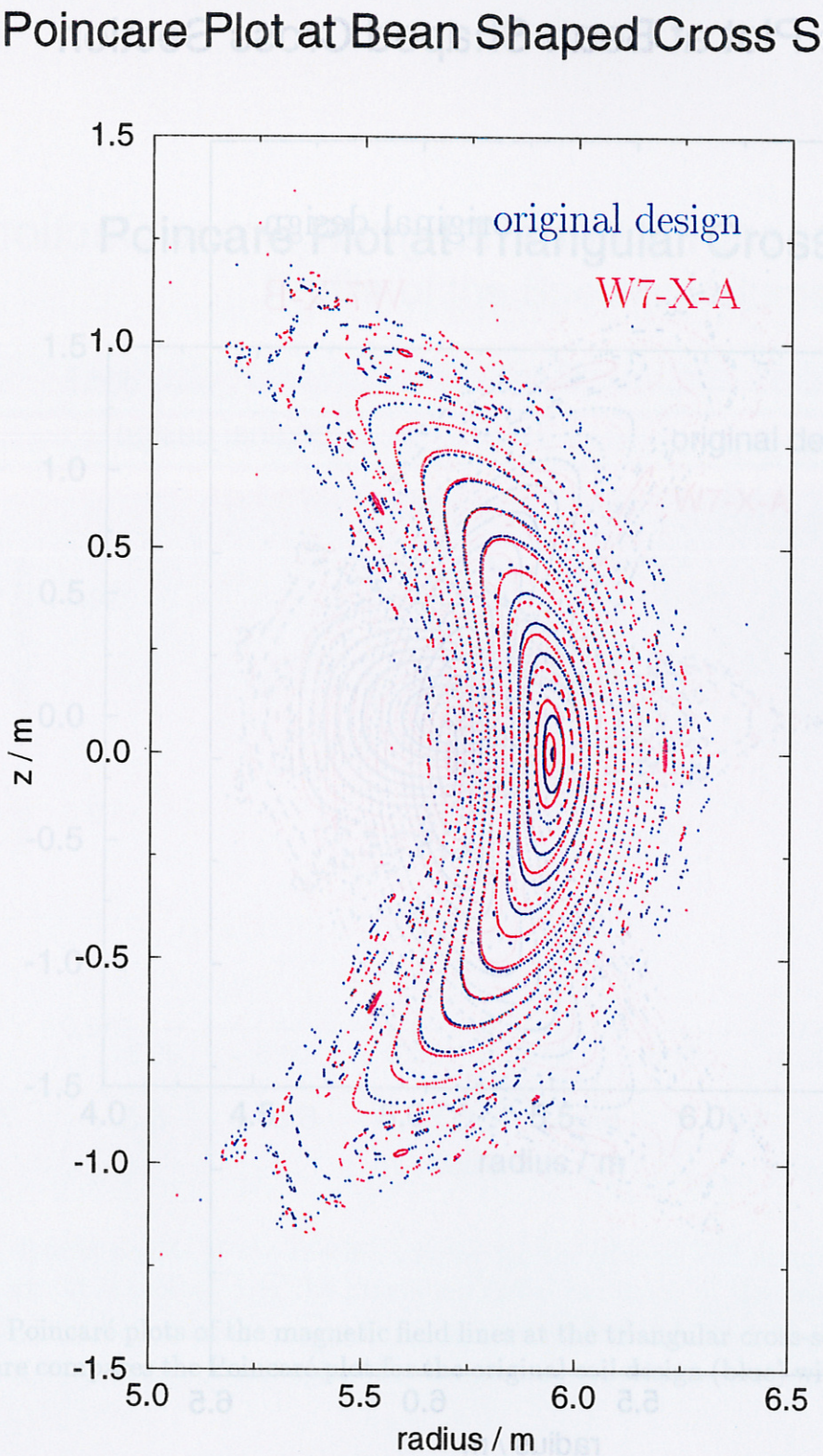

Fig. 8: Poincaré plots of the magnetic field lines at the bean shaped cross-section of the machine. The figure compares the Poincaré plot for the original coil design (blue) with the W7-X-A design (red).

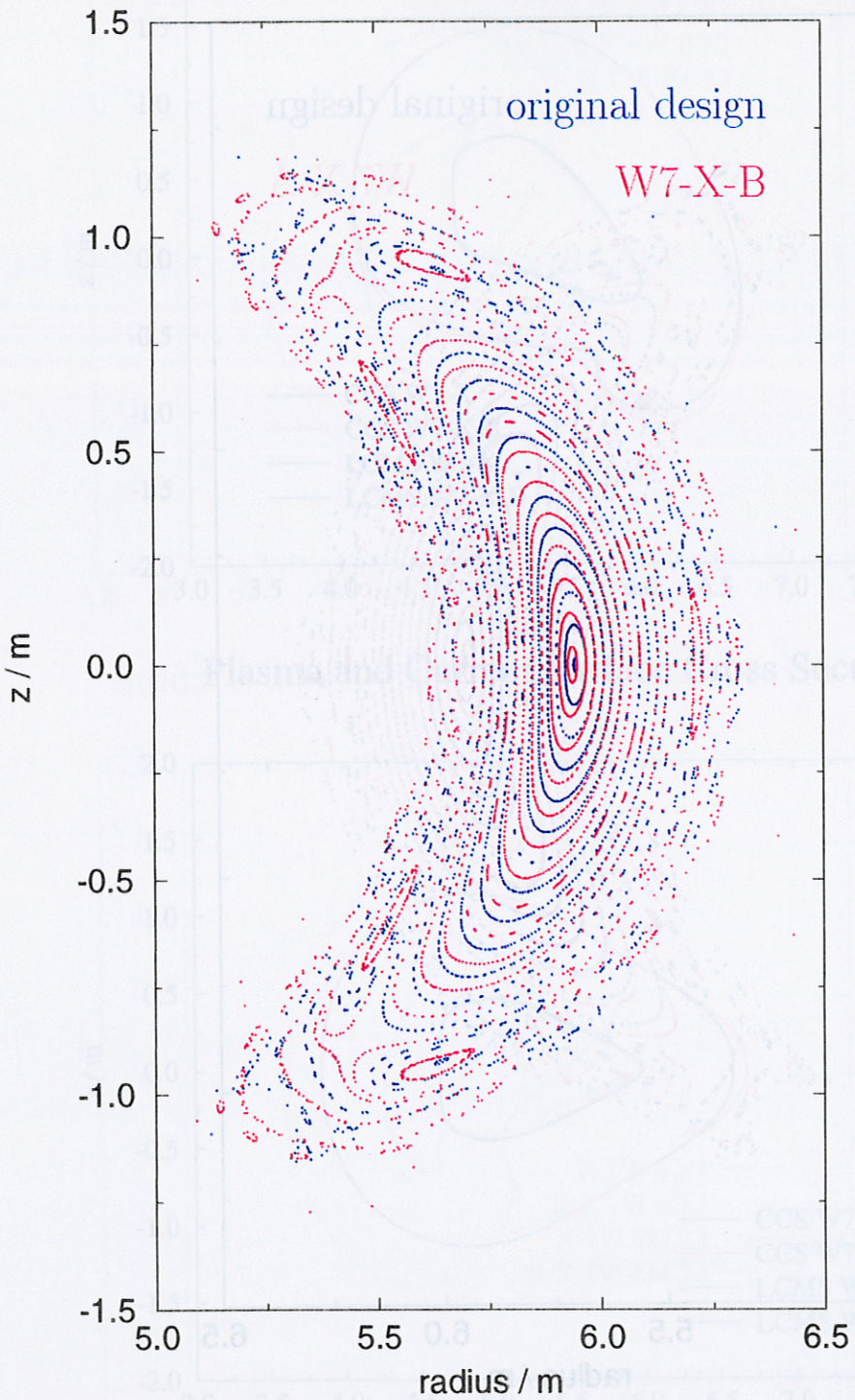

Fig. 9: Poincaré plots of the magnetic field lines at the bean shaped cross-section of the machine. The figure compares the Poincaré plot for the original coil design (blue) with the W7-X-B design (red).

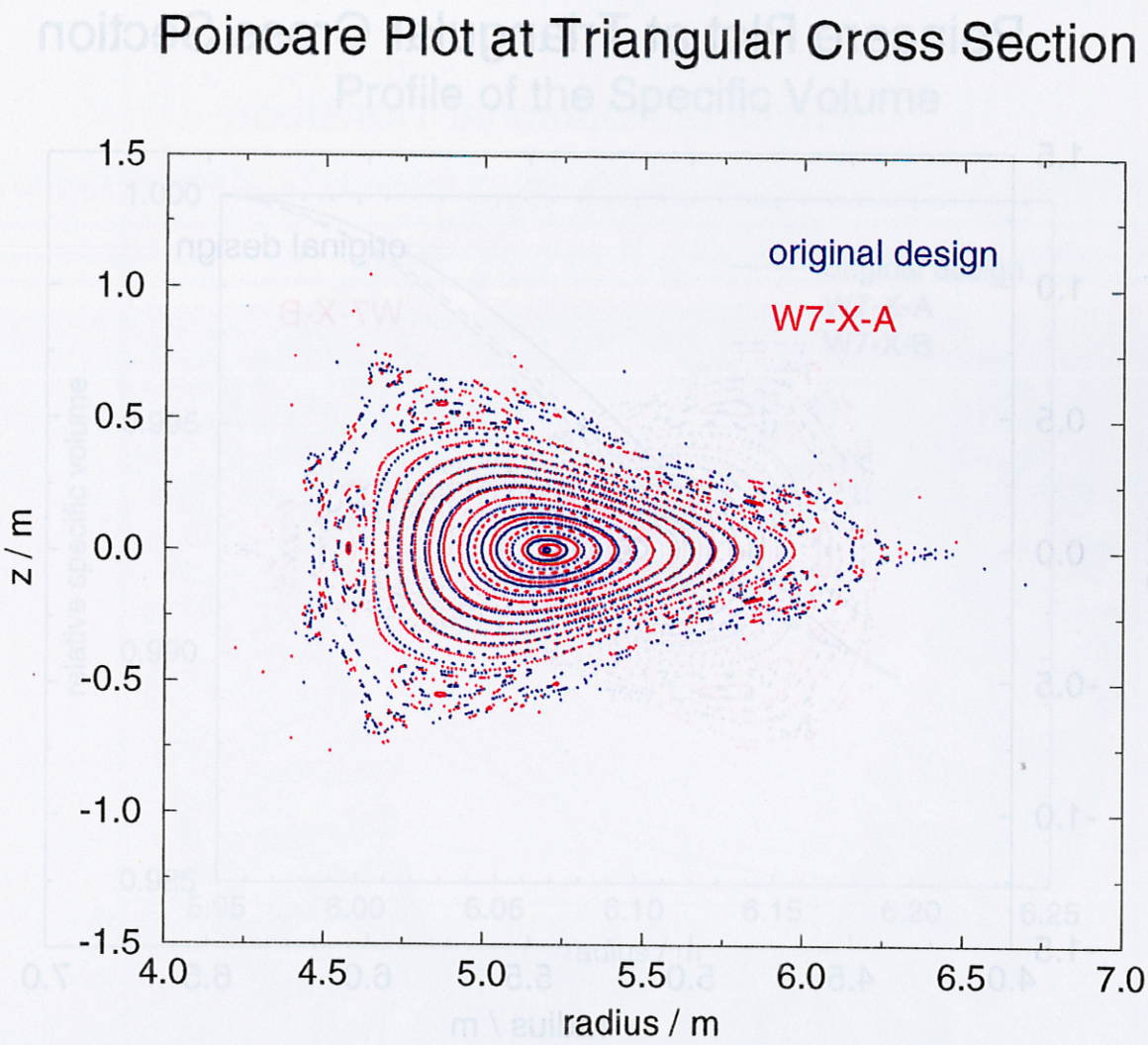

Fig. 10: Poincaré plots of the magnetic field lines at the triangular cross-section of the machine. The figure compares the Poincaré plot for the original coil design (blue) with the W7-X-A design (red).

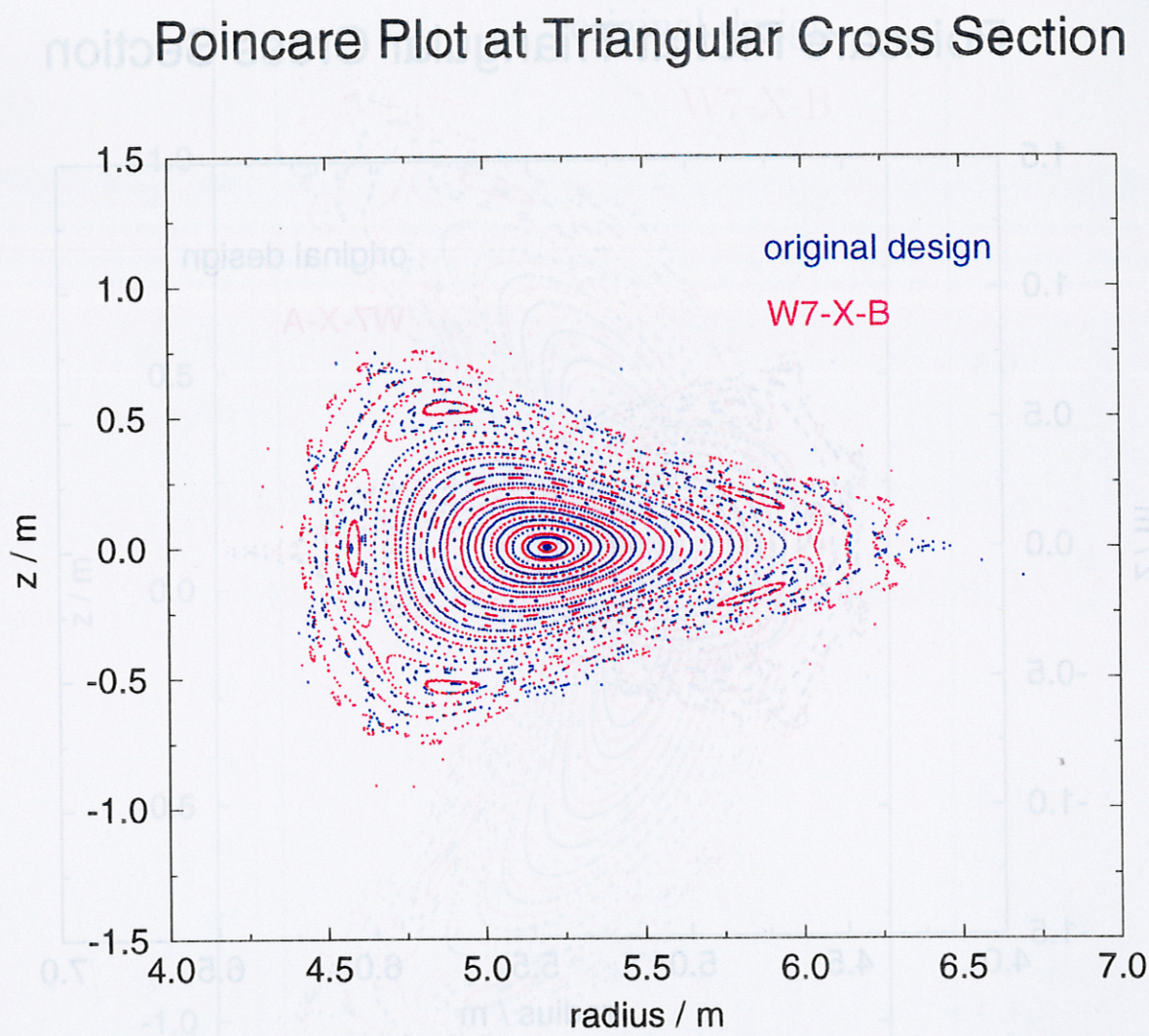

Fig. 11: Poincaré plots of the magnetic field lines at the triangular cross-section of the machine. The figure compares the Poincaré plot for the original coil design (blue) with the W7-X-B design (red).

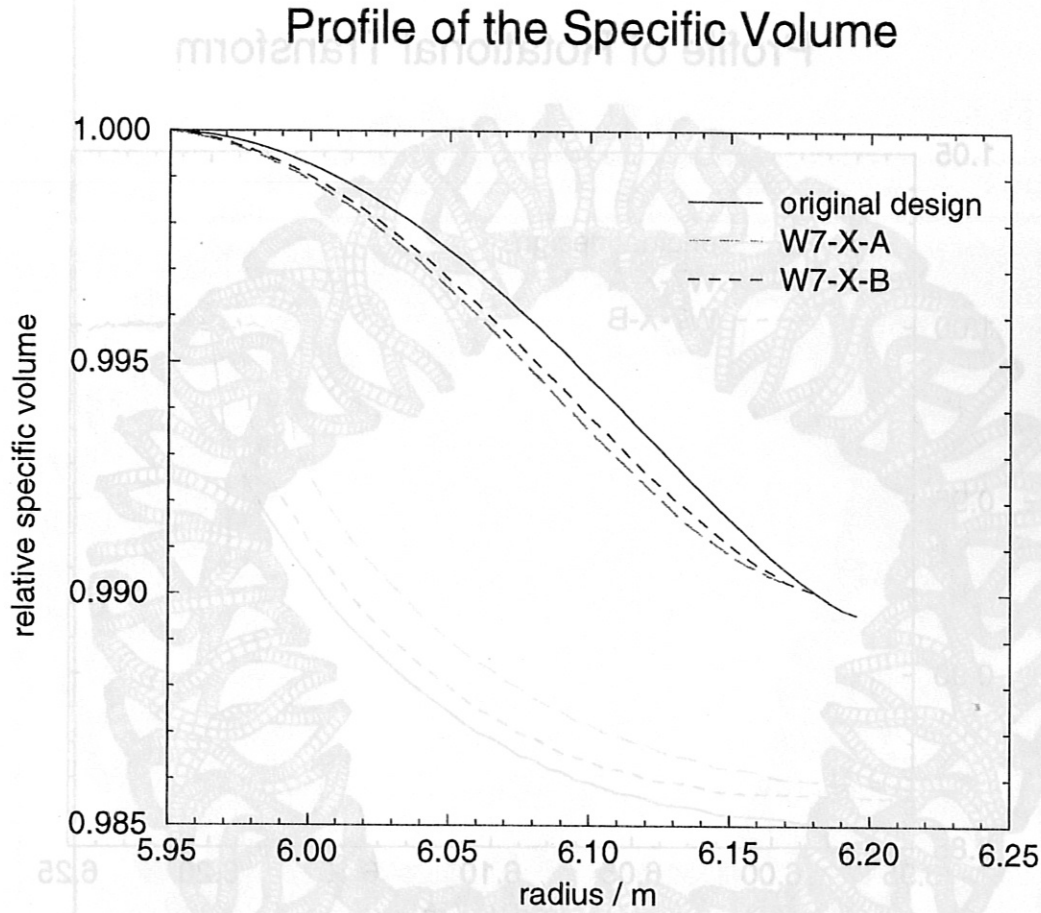

Fig. 12: Radial profile of the specific volume for the present coil design and for the new optimizations. It is plotted over the maximum radial excursion of the field lines encountered in the bean shaped cross-section. The values are normalized to their peak values on the magnetic axis.

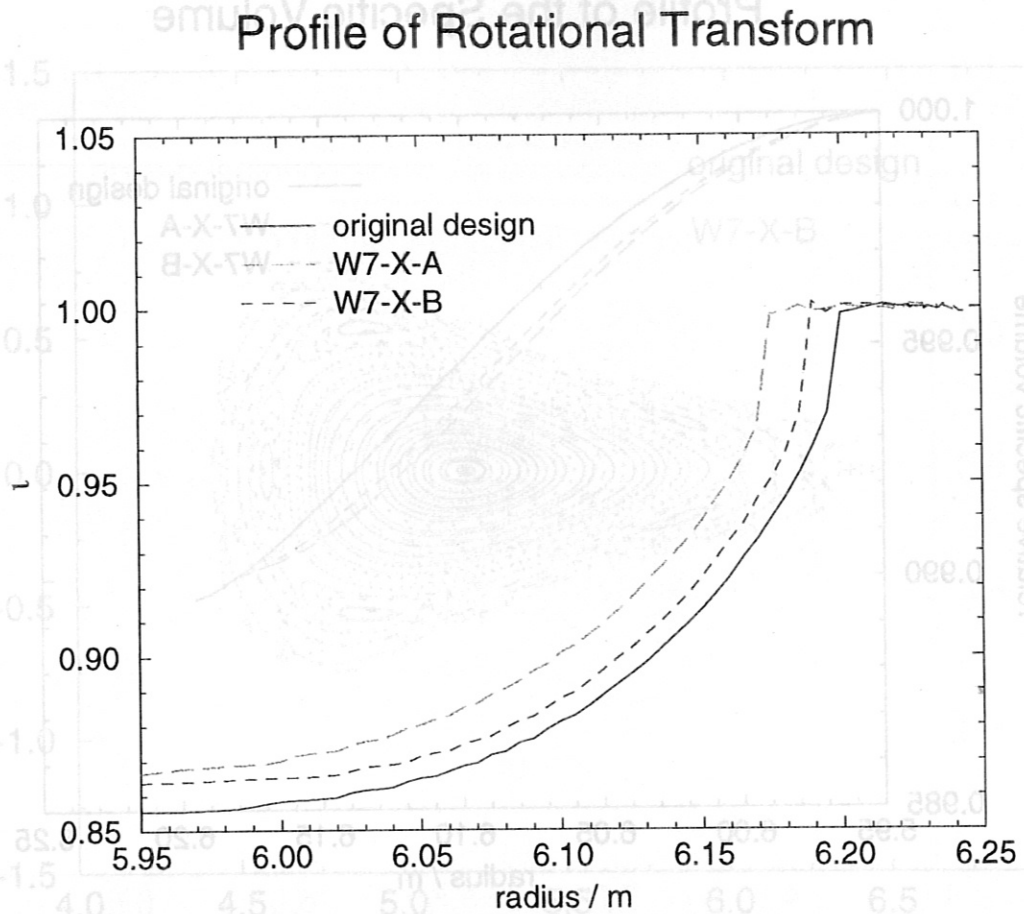

Fig. 13: Radial profile of the rotational transform ι for the present coil design and for the new optimization. It is plotted over the maximum radial excursion of the field lines encountered in the bean shaped cross-section.

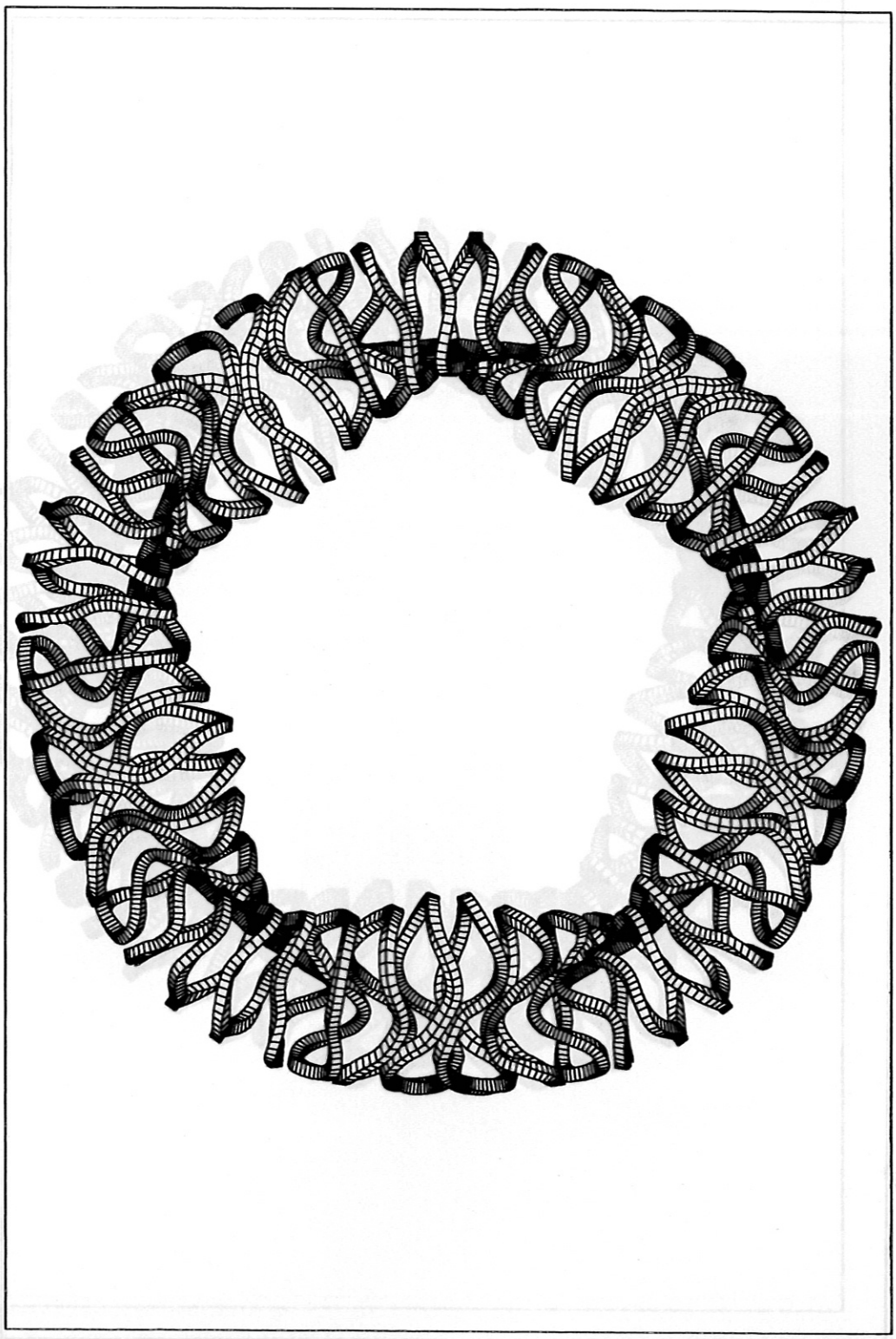

Fig. 14: Top view of the complete coil system, case W7-X-A.

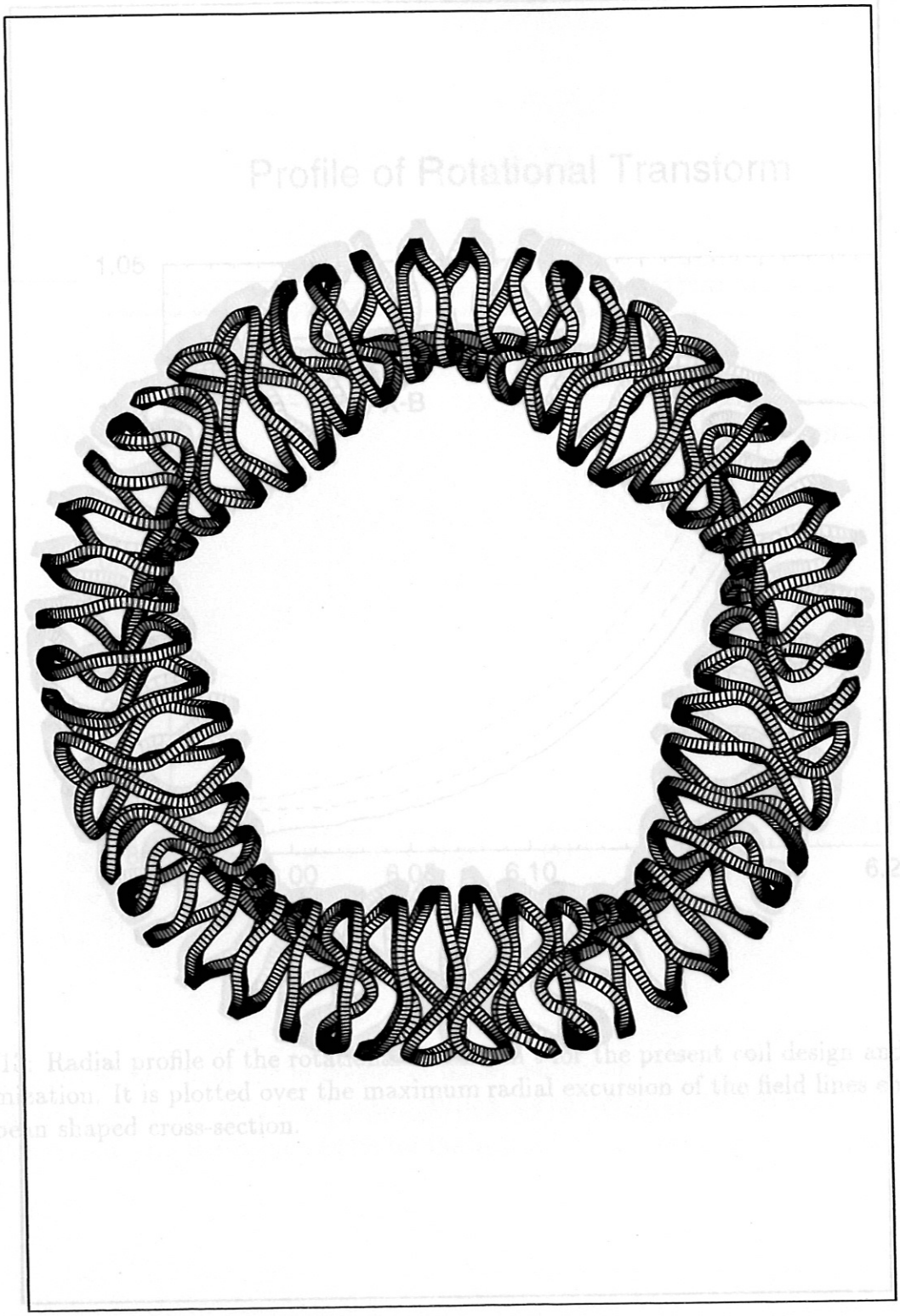

Fig. 15: Top view of the complete coil system, case W7-X.

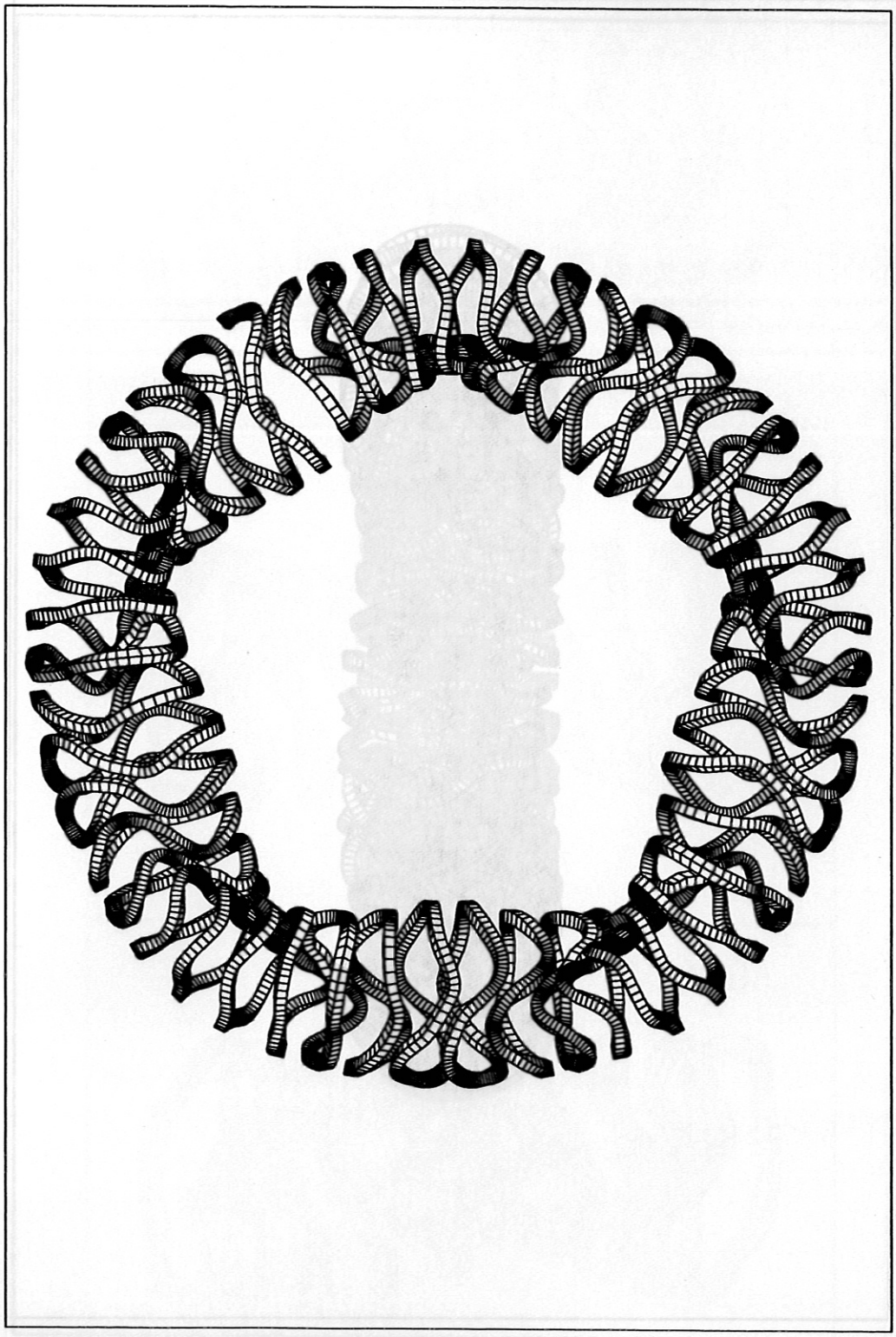

Fig. 16: Top view of the complete coil system, case W7-X-B.

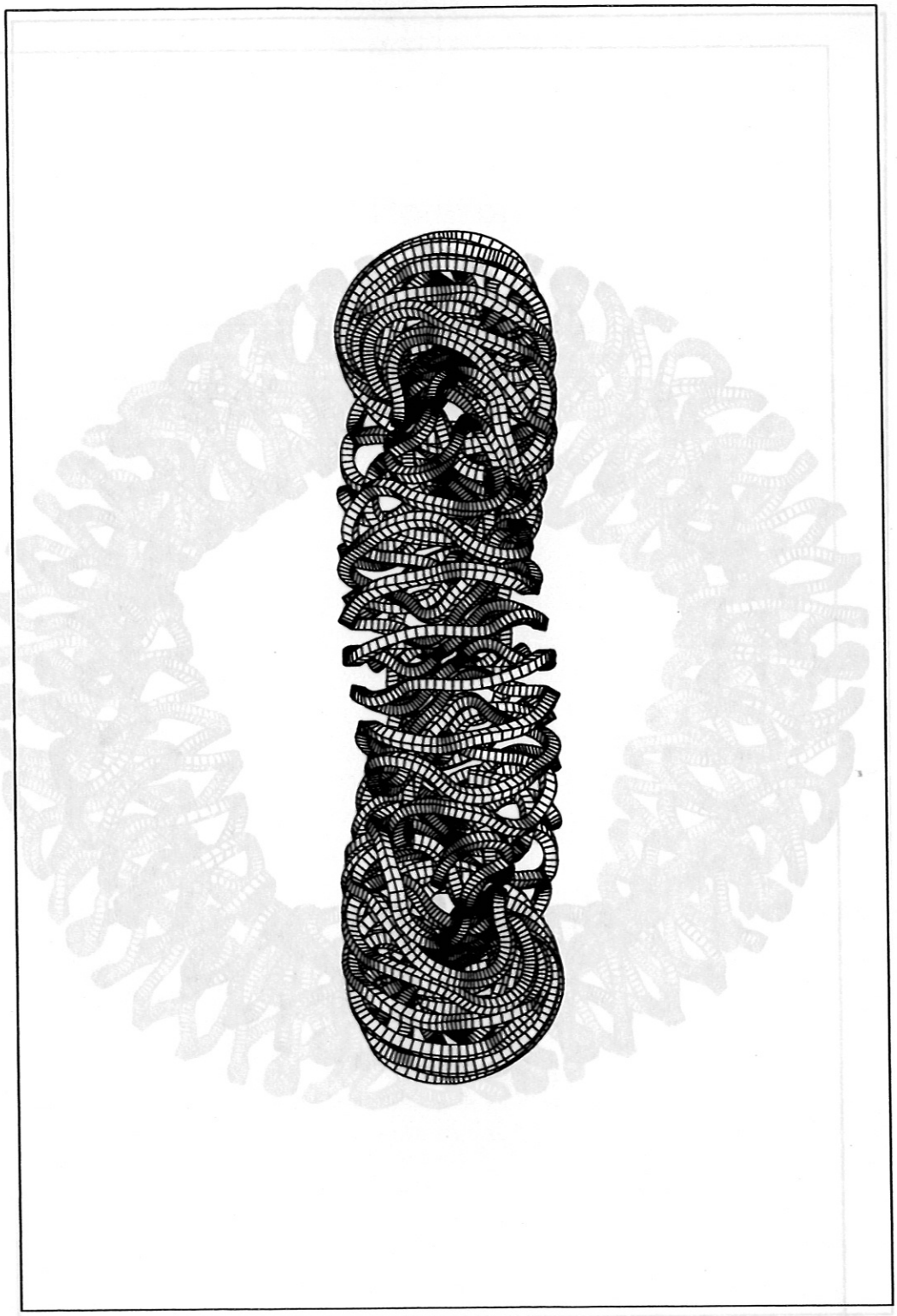

Fig. 17: Side view of the complete coil system, case W7-X-A. The figure is tilted for greatest magnification.

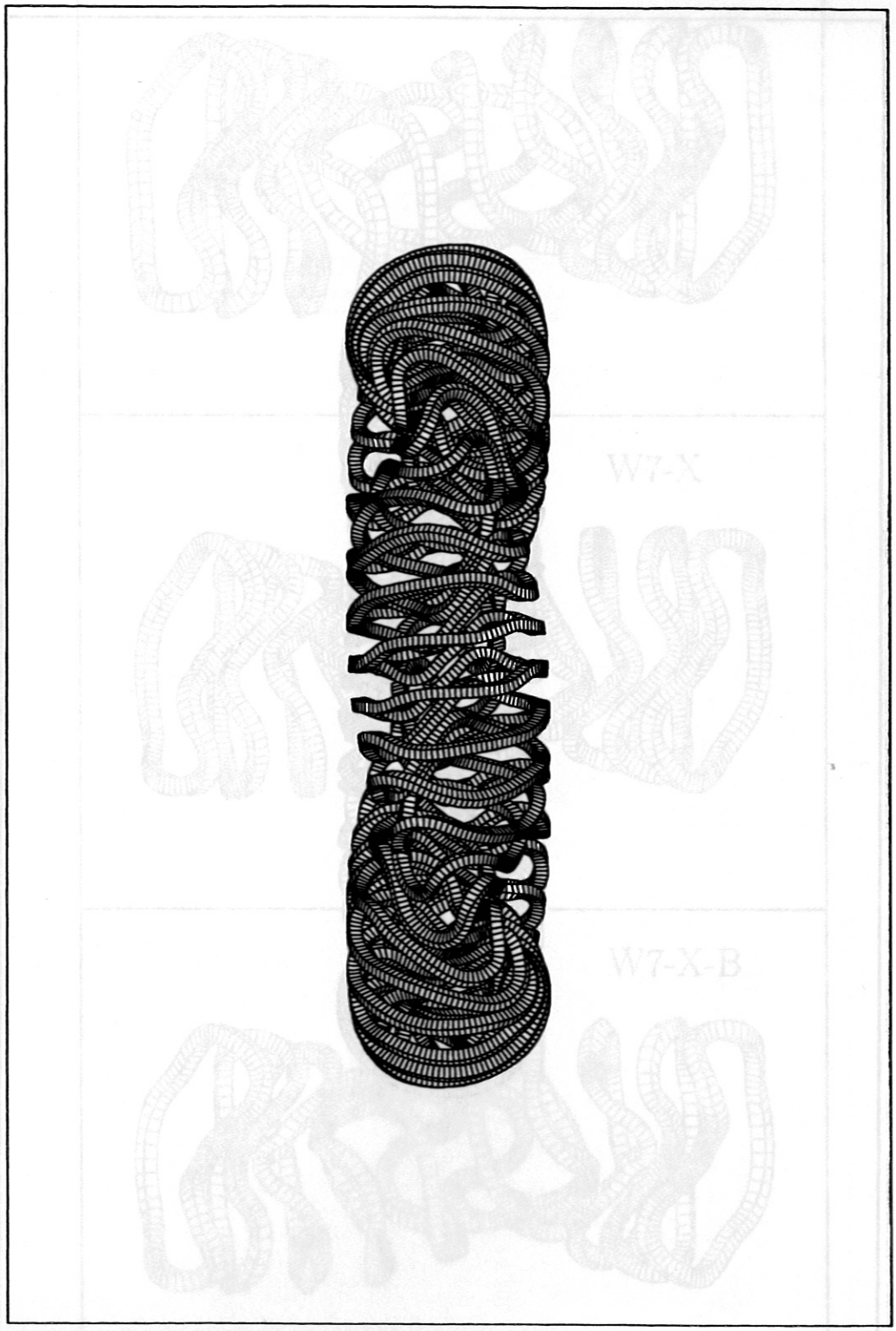

Fig. 18: Side view of the complete coil system, case W7-X. The figure is tilted for greatest magnification.

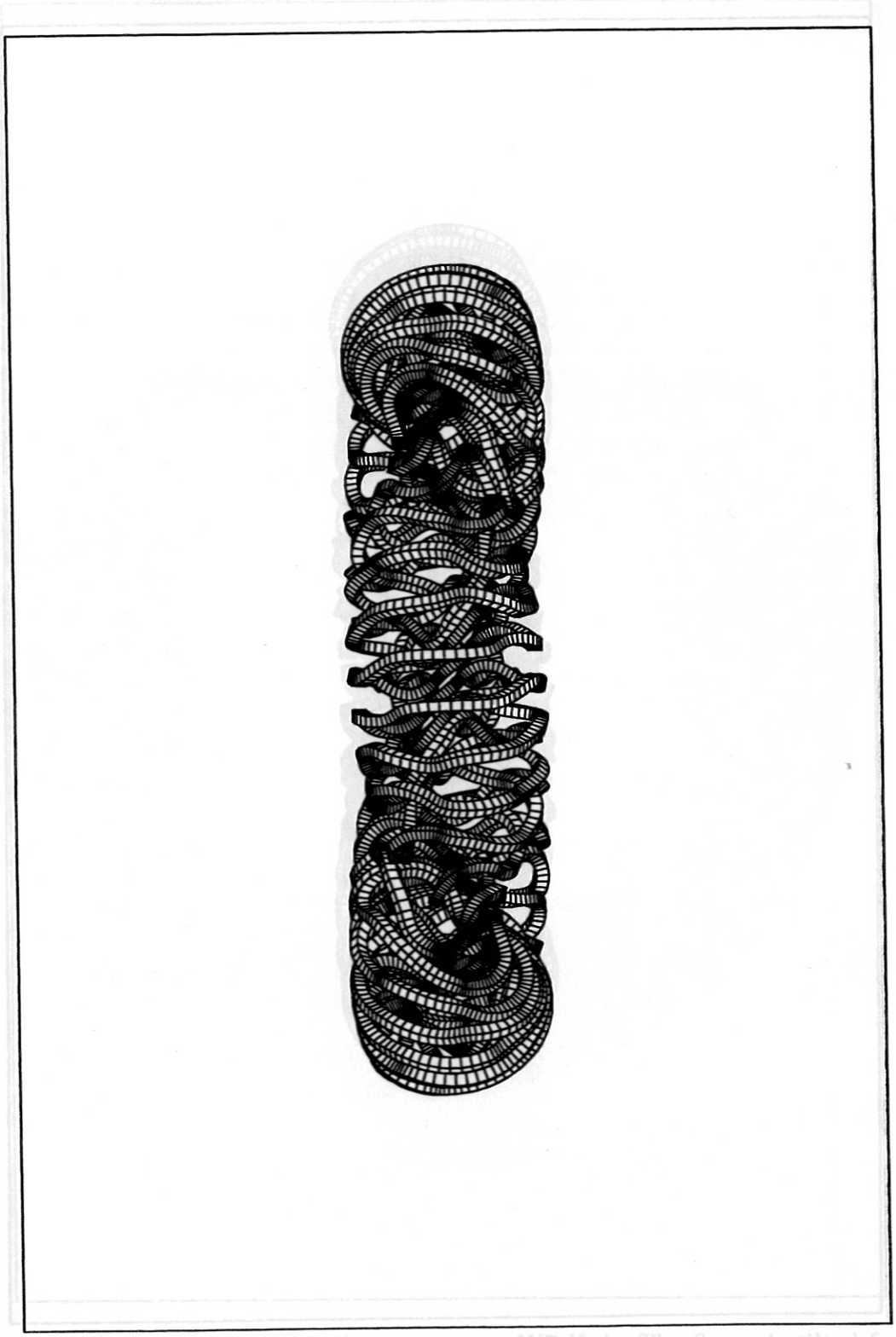

Fig. 19: Side view of the complete coil system, case W7-X-B. The figure is tilted for greatest magnification.

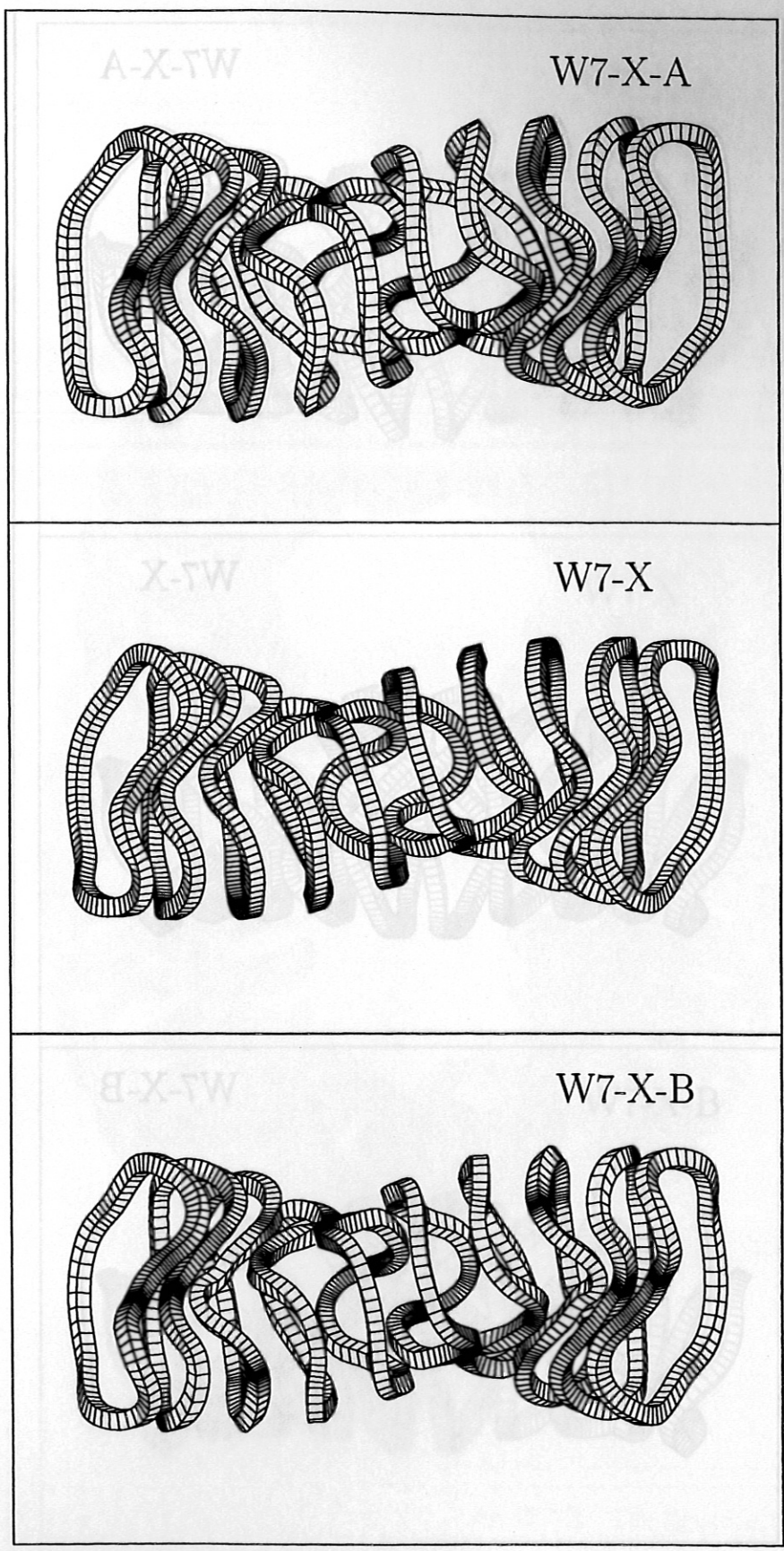

Fig. 20: Inner view of one period of the coil system. The figure compares the original design as from jan. 1996 (center) with the case W7-X-A (top) and W7-X-B (bottom).

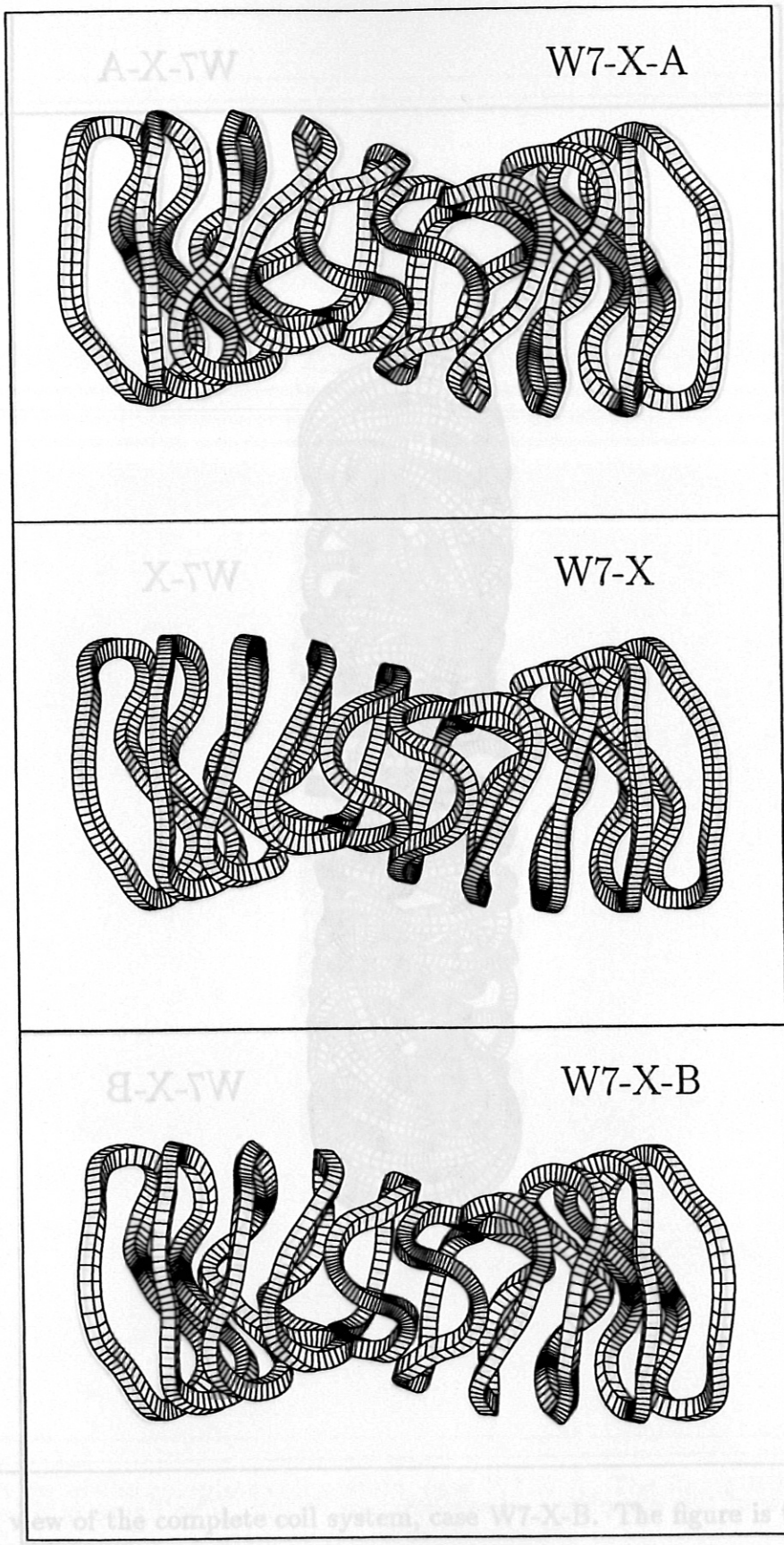

Fig. 21: Outer view of one period of the coil system. The figure compares the original design as from jan. 1996 (center) with the case W7-X-A (top) and W7-X-B (bottom).

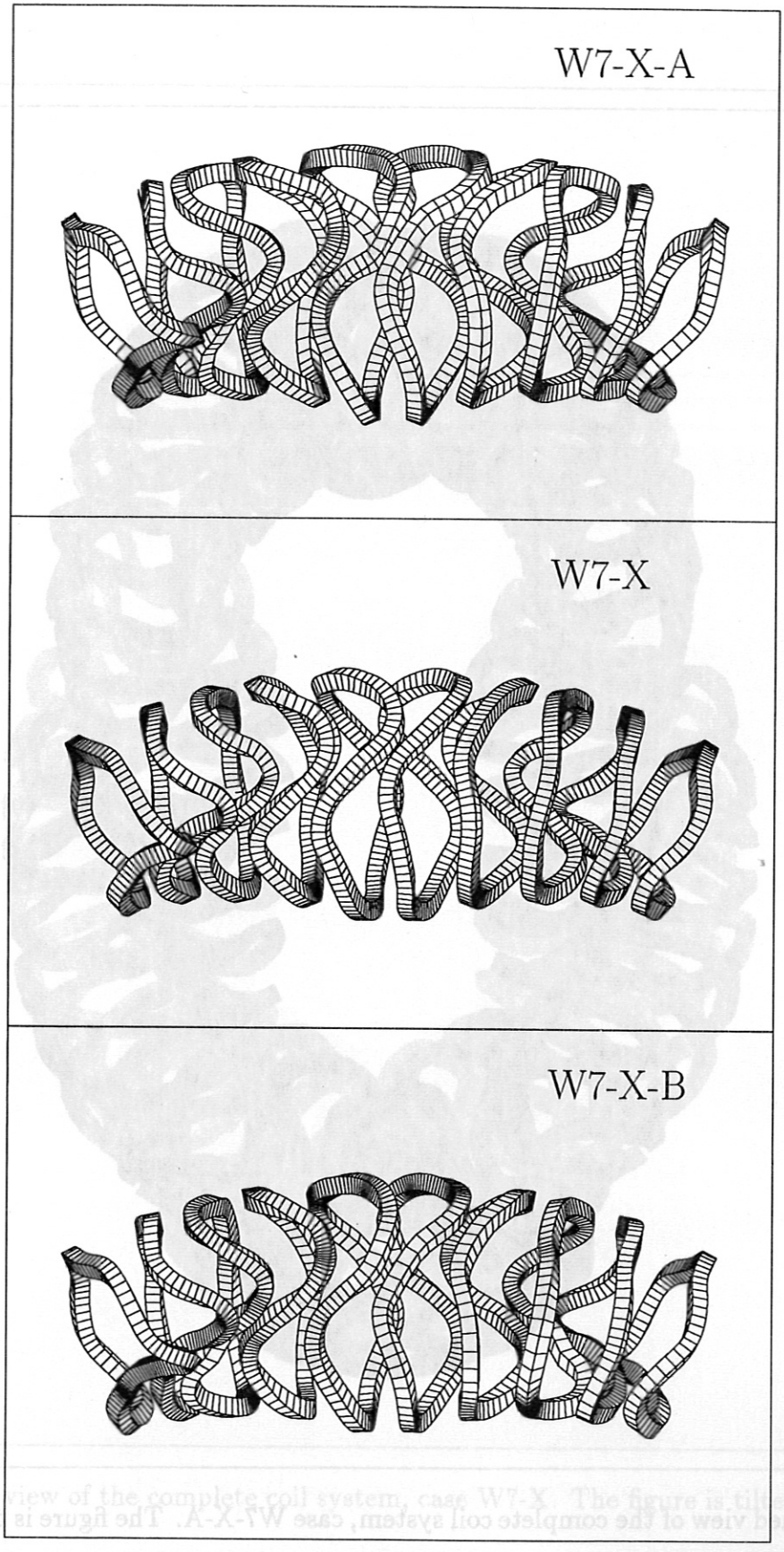

Fig. 22: Top view of one period of the coil system. The figure compares the original design as from jan. 1996 (center) with the case W7-X-A (top) and W7-X-B (bottom).

Fig. 23: Inclined view of the complete coil system, case W7-X-A. The figure is tilted for greatest magnification.

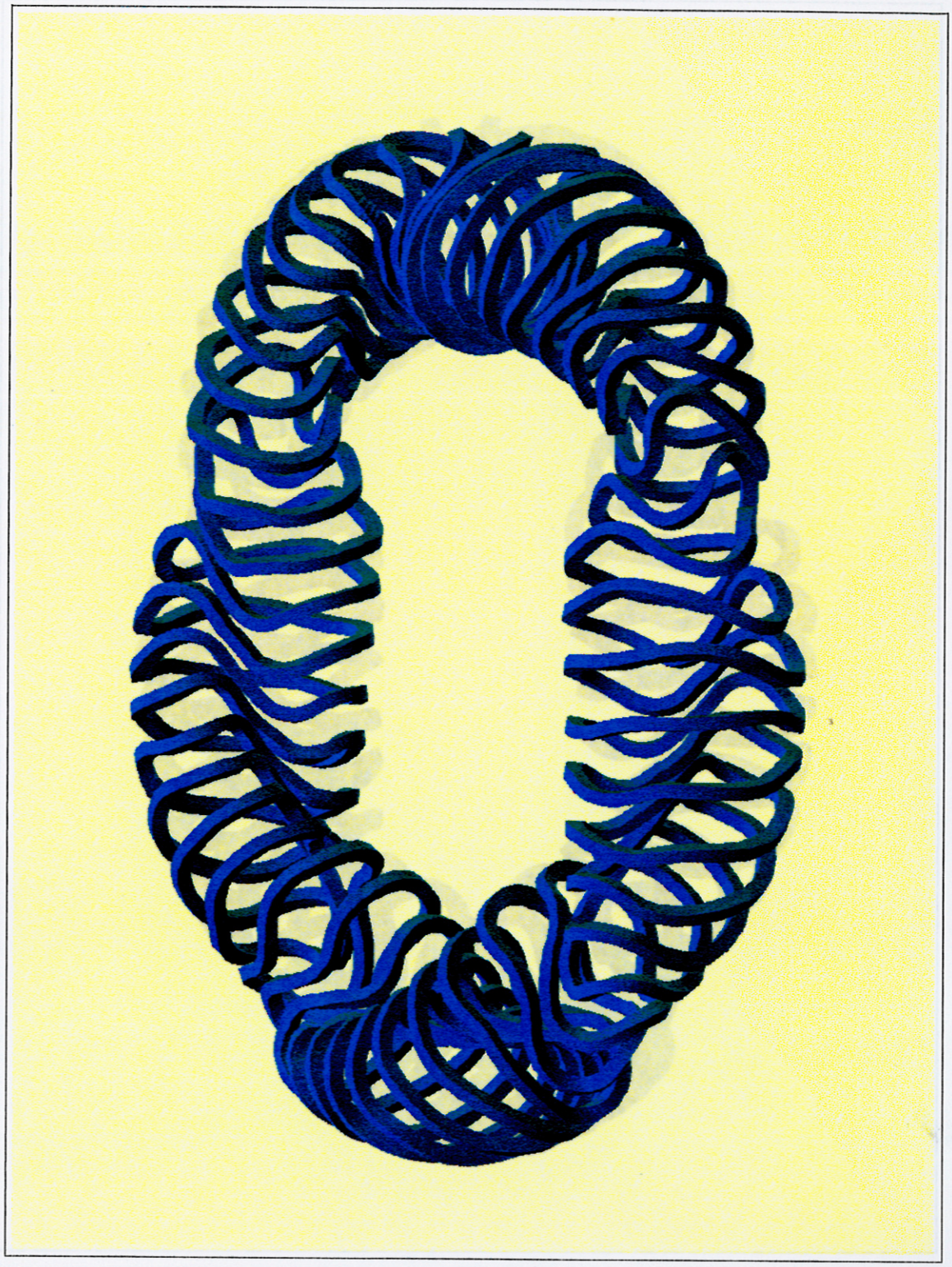

Fig. 24: Inclined view of the complete coil system, case W7-X. The figure is tilted for greatest magnification.

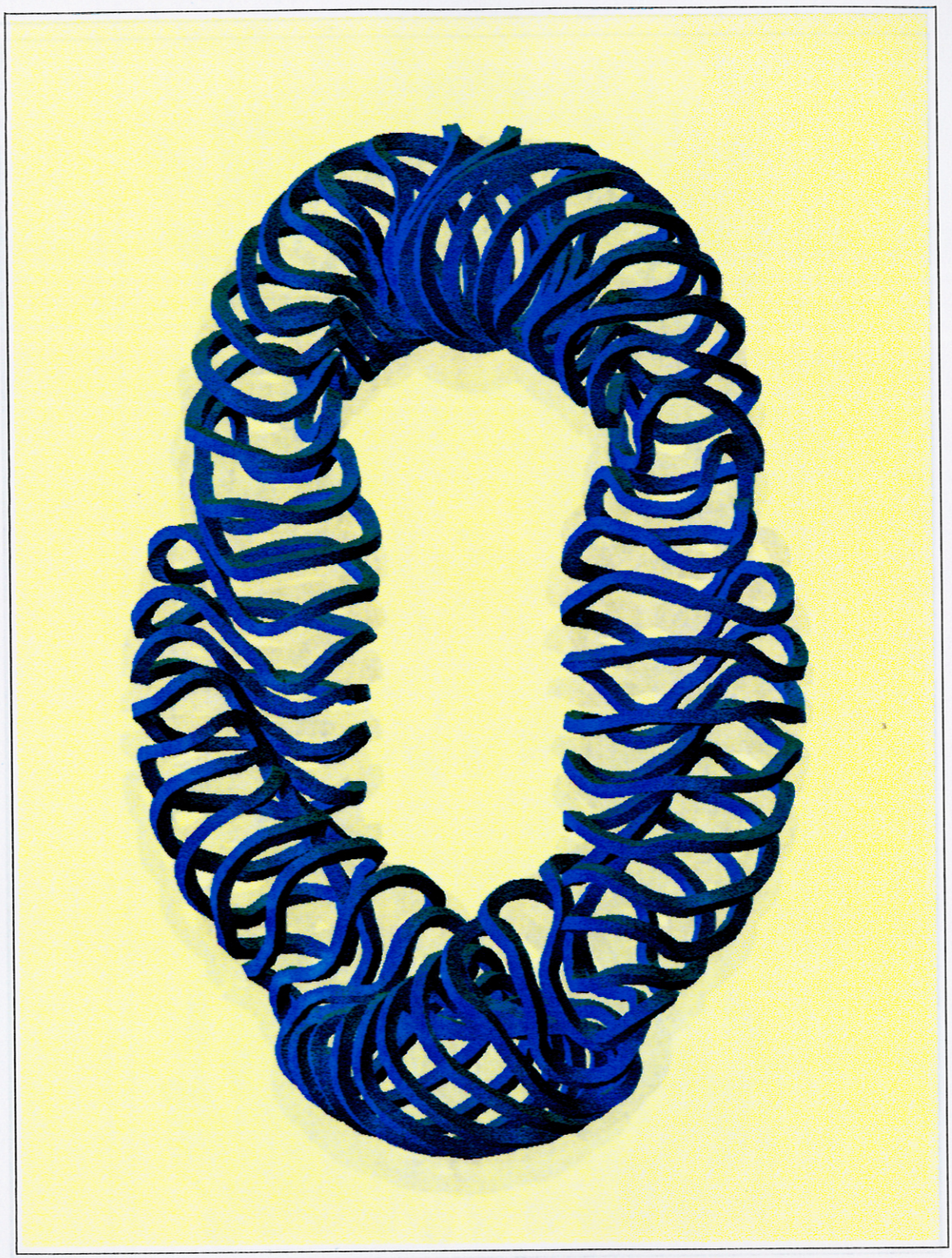

Fig. 25: Inclined view of the complete coil system, case W7-X-B. The figure is tilted for greatest magnification.